Wiley
Journal of Food Biochemistry
Volume 2025, Article ID 8353971, 18 pages
https://doi.org/10.1155/jfbc/8353971

WILEY

Research Article

Antioxidant Activity of Pressafonin-A Isolated From Sicilian *Ferulago nodosa* (L.) Boiss. Roots and Its Proapoptotic Effect Through ROS-Dependent p53/p21$^{Waf1/Cip1}$ Pathway in Human Melanoma A-375 Cells

Ignazio Restivo,[1] **Natale Badalamenti**,[1,2] **Maurizio Bruno**,[1,2,3] **Ilenia Concetta Giardina**,[1] **Alessandro Massaro**,[1] **Mario Allegra**,[1] **Luisa Tesoriere**,[1] **and Alessandro Attanzio**[1]

[1]*Department of Biological, Chemical and Pharmaceutical Sciences and Technologies (STEBICEF), University of Palermo, Palermo 90128, Italy*
[2]*NBFC-National Biodiversity Future Center, Piazza Marina 60, Palermo 90133, Italy*
[3]*Centro Interdipartimentale di Ricerca "Riutilizzo Bio-Based Degli Scarti da Matrici Agroalimentari" (RIVIVE), University of Palermo, Viale Delle Scienze, Palermo 90128, Italy*

Correspondence should be addressed to Natale Badalamenti; natale.badalamenti@unipa.it and Luisa Tesoriere; luisa.tesoriere@unipa.it

Received 23 October 2024; Accepted 22 May 2025

Academic Editor: Xiaoyu Song

Ferulago nodosa (L.) Boiss. is a species belonging to the Apiaceae family which grows spontaneously in the Balkan and southern Tyrrhenian areas of the Mediterranean Sea. Plants of the *Ferulago* genus are widely used in the ethnopharmacological field, mainly in the form of infusions, as remedies against panic attacks, to solve problems related to the gastrointestinal tract, and for ulcer complications. In this study, we assessed antioxidant and antiproliferative activities of the pressafonin-A (PA), extracted from *F. nodosa* roots, following its spectroscopical characterization. Among the assays conducted, reducing capacity tests and free radical scavenging assays showed that PA can act as an antioxidant. PA also exhibited time- and concentration-dependent antiproliferative activity against human cancer cell lines, including A-375 (melanoma), HCT-116 (colorectal carcinoma), and MCF-7 (breast adenocarcinoma). Selectivity index (SI) was calculated using normal 16-HBE cells. Among the cell lines tested, PA demonstrated an SI > 10 in A-375 cells. Treatment with PA 6.2 μM (IC_{25}) and 12.4 μM (IC_{50}) for 24-h induced apoptosis, as cytofluorimetrically evidenced by phosphatidylserine exposure, loss of mitochondrial membrane potential, and intracellular ROS production. Moreover, PA caused an arrest of cell cycle at the G1/S phase transition. Western blot analysis showed that PA caused an increase in protein levels of p53, p21$^{Waf1/Cip1}$, cytochrome c, and BAX, along with a decrease in Bcl-2 protein. In conclusion, natural PA demonstrated antioxidant and antiproliferative properties on A-375 by inducing apoptosis via ROS-dependent intrinsic mitochondrial pathway and cell cycle arrest. These results suggest that PA may have potential as a chemopreventive agent for skin diseases.

Keywords: antiproliferative; apoptosis; cell death; *Ferulago nodosa* (L.) Boiss.; human melanoma cells; pressafonin-A

1. Introduction

The genus *Ferulago* W.D.J.Koch, belonging to the Apiaceae family, consists of 48 currently accepted species distributed in all the countries bordering the Mediterranean Sea (except Libya, the Spanish islands, and Sardinia), and in the territories between southern Russia and Iran [1]. Present day Turkey has been identified as a center of diversification of this genus given the important presence of 34 of the 48 species accepted in the world [1, 2].

In Sicily, this genus consists of only two species, *Ferulago nodosa* (L.) Boiss. and *Ferulago galbanifera* (Mill.) W.D.J.Koch, both botanically grouped in the subgenus Galbanifera [2]. Between the two, *F. nodosa*, the object of this work, has a clear Balkan–Tyrrhenian distribution, being present only in the territories of the old Yugoslavia, Greece, and in Western Sicily, in the Noto Valley (Italy) [1].

A study based on the geographical isolation of this accession and on its morphological characteristics [3] proposed assigning the name of the subspecies *F. nodosa* subsp. *geniculata* (Guss.) [4], but this, at the moment, remains only an intraspecific species of *F. nodosa.*

Ferulago genus is widely recognized and above all used in traditional medicine [5], for example, in the treatment of physiological problems related to the gastrointestinal tract [6], or for the treatment of ulcers [7]. Furthermore, several studies are reported for the use of species as a sedative [8], for hemorrhoid diseases [9], and for skin care [10]. However, many species, once dried, are used as natural preservatives for various foods, such as cheese [11] and meat [12].

Most of the investigated biological activities, such as antimicrobial [13], antifungal [14, 15], antioxidant [16, 17], cytotoxic [18, 19], hepatoprotective [20], and nephroprotective [21], on the extracts and on essential oils of many *Ferulago* species, are caused by the wide structural diversity of secondary metabolites present in the various plants' parts (roots, leaves, flowers, and branches). Phytochemically, the main metabolite class is composed by different coumarins (1,2-benzopyrone). It has been observed that all isolated furanocoumarins are all biogenetically linear, and not angular, and very often esterified with a prenyl moiety or with an aromatic ring [5]. These compounds are found in considerable quantities in the root systems and are the most studied metabolites to evaluate their in vivo anticoagulant properties. In addition, several flavonoids [22], terpenoids [23], ferulol products [24, 25], and cinnamic acid derivatives [26] have been identified.

A metabolite resulting from the biosynthetic combination of the shikimic and the mevalonic acid pathway, pressafonin-A (PA), isolated from the roots of the Sicilian population of *F. nodosa*, has never been reported so far as occurrence in the *Ferulago* genus. It is a compound already isolated from *Bolax gummifera* [27], *Chloranthus elatior* [28], *Cistus libanotis* [29], *Coreopsis mutica* [30], *Eupatorium deltoideum* [31], *Hedyosmum scabrum* [32], *Illicium verum* [33], *Magnolia biondii* [34], *Magnolia maudiae* [35], *Michelia compressa* var. *formosana* [36], *Pinus pumila* [37], *Piper cernuum* [38], *Valeriana wallichii* [39], *Verbesina rupestris* [40], *Verbesina sphaerocephala* [41], and *Verbesina turbacensis* [42]. PA has demonstrated interesting activities, such as antimicrobial against *Staphylococcus aureus* (MIC_{90} 25 μM) [37, 43], moderate antileishmanial activity against *Leishmania major* promastigotes in vitro (IC_{50} 12.2 μM) and cytotoxicity against macrophages (J774.1 murine cell line) (IC_{50} 8.6 μM) [39], and excellent antiviral activity against influenza virus A/Puerto Rico/8/34 H1N1 (PR8) (IC_{50} 1.7 μM) [33].

Naturally derived compounds have attracted considerable attention due to their antioxidant and antiproliferative activities, supporting their potential in disease prevention and cancer therapy [44]. These compounds can scavenge reactive oxygen species (ROS) and modulate redox-sensitive signaling pathways, thereby enhancing cellular antioxidant defenses and reducing oxidative damage under physiological conditions [45]. In contrast, in tumor cells, many of these molecules exert antiproliferative effects by inducing oxidative stress, cell cycle arrest, or apoptosis through mitochondrial dysfunction or inhibition of key survival pathways such as PI3K/Akt or NF-κB [46, 47]. This dose- and context-dependent behavior supports the therapeutic versatility of natural bioactives as both protectants in normal cells and cytotoxic agents in malignancy [48].

Building on these observations and given the growing interest in studying phytochemicals from the Mediterranean region, this study aimed to evaluate the antioxidant capacity in vitro and antiproliferative activity of PA on different cancer cells, deepening the pathways involved in its apoptotic effect on human melanoma A-375 cells.

2. Experimental Procedures

2.1. Chemicals. Unless otherwise specified, all reagents and chemicals were purchased from Merck (Milan, Italy) and are of the highest available purity grade. Merck No. 7734 silica gel, deuterated chloroform, formic acid, water, methanol, acetone, petroleum ether, ethyl ether, anisaldehyde, and sulfuric acid were purchased from Sigma-Aldrich (Via Monte Rosa, 93, 20,149 Milan, Italy) and were used without further purifications.

2.2. General Experimental Procedures. Silica gel (70–230 mesh AsTM) deactivated with 15% water was used for column chromatography. A Coolsafe 4–15-L freeze dryers tool with a capacity of 4 L was used for freeze drying. The characterization of PA was carried out by ^{1}H-NMR and ^{13}C-NMR spectroscopy with a Bruker Avance II spectrometer with a rotating MAs probe at 15 KHz operating at 400 MHz for recording the ^{1}H-NMR spectra, and at 100 MHz for the ^{13}C spectra, at the Large Equipment Center of the University of Palermo. DEPT, ^{1}H-^{1}H-COSY, HMBC, HSQC, and NOESY experiments were performed using Bruker microprograms and tetramethylsilane (TMS) was used as internal standard. The sample to be analyzed was brought into solution with $CDCl_3$. For all spectra, the chemical shifts (δ) are expressed in ppm and the coupling constants J are expressed in Hz. The sample was also subjected to Agilent 1260 Infinity HPLC-MS analysis. A Zorbax Extend C_{18} reversed column (2.1 × 50 mm, 1.8 μm particle size), with Phenomenex C_{18} safety column

(4 × 3 mm), was used. The flow rate was 0.5 mL/min, and the column temperature was set to 25°C. The eluents formic acid/water were in Phase A and formic acid/methanol in Phase B. The injection volume was 3 μL. Everything was monitored by MS-TIC. Mass spectrum was obtained with the Agilent 6540 UHD accurate mass Q-ToF spectrometer equipped with an AJS ESI dual working resource operating in positive mode and in negative mode. N_2 was used as a desolvating gas at 320°C with a flow rate of 10 L/min. The nebulizer was set at 35 psig. The jacket gas temperature was set at 350°C with a flow rate of 11 L/min. A potential of 3.5 kV on the capillary was used for the positive ion mode. The fragmenter was selected at 75 V. The mass spectrum was recorded in the 100–1000 m/z range. Polarimetric measurement was performed for the determination of the stereochemistry. A Jasco P1010 digital polarimeter was used for this analysis.

2.3. Plant Materials. *F. nodosa* plants, in full flowering stage, were collected in May 2023 in the immediate vicinity of the city of Noto, Syracuse (Italy) (36°48′21.22″ N; 15°01′14.67″ E) at 280 m above sea level. Some specimens (Voucher PAL 111076), collected and identified by Prof. Vincenzo Ilardi, were deposited at the Herbarium Mediterraneum Panormitanum of the Botanical Garden of the University of Palermo, Italy.

2.4. Isolation of PA. The roots of *F. nodosa* (300 g), manually separated from the aerial parts, were washed in distilled water, cut into thin pieces, and frozen at −20°C. Subsequently, they were subjected to a freeze-drying cycle to eliminate all the water present, obtaining 80 g of dry material. The solid obtained was then finely crushed through a ceramic mortar and extracted with acetone (0.5 L × 3 times) at room temperature and in the dark room. After appropriate filtration, the solvent was evaporated at reduced pressure and at temperatures below 40°C. The obtained extract (6 g) was subjected to column chromatography using silica gel deactivated with 15% of cold water as the stationary phase, and the mixtures in the ratio 5:5, 3:7, 2:8, and 1:9 v/v as eluent to provide eight different fractions (Fn1-Fn8). The general anisaldehyde/H_2SO_4 system was used as the detection system on TLC. Fn6 (27 mg) was purified by silica gel (petroleum ether/ethyl ether 2:8, v/v) to afford PA (11.7 mg). The isolated PA was finally dissolved in dimethyl sulfoxide (DMSO), aliquoted, and stored at a concentration of 100 mM for use in all subsequent in vitro assays.

2.5. Physical Property of PA. Yellow powder; $(\alpha)_D^{25}$ −4.1 (c = 0.50, $CHCl_3$); IR: ν_{max} 3411, 1665, 1589, 1448, 1154, and 918 cm^{-1}; HPLC-ESI/MS: m/z 323.1638 $(M + Na)^+$ (calcd. for $C_{19}H_{24}NaO_3$, 323.1628 Da); ^{1}H-NMR (400 MHz, $CDCl_3$-d): δ_H 7.63 (1H, d, J = 15.8 Hz, H-2), 6.33 (1H, d, J = 15.8, H-3), 7.44 (1H, d, J = 8.8 Hz, H-5), 6.87 (1H, d, J = 8.8 Hz, H-6), 6.87 (1H, d, J = 8.8 Hz, H-8), 7.44 (1H, d, J = 8.8 Hz, H-9), 5.02 (1H, ddd, J = 9.6, 3.6, 2.0 Hz, H-2′), 1.07 (1H, m, H-3′a), 2.42 (1H, m, H-3′b), 1.71 (1H, t, J = 4.6 Hz, H-4′), 1.32 (1H, m, H-5′a), 1.79 (1H, m, H-5′b), 1.36 (1H, m, H-6′a), 2.05 (1H, m, H-6′b), 0.94 (3H, s, H-8′), 0.90 (3H, s, H-9′), 0.89 (3H, s, H-10′); ^{13}C-NMR (100 MHz, $CDCl_3$-d): δ_C 168.09 (C-1), 116.02 (C-2), 144.20 (C-3), 127.17 (C-4), 129.94 (C-5), 115.89 (C-6), 157.92 (C-7), 115.89 (C-8), 129.94 (C-9), 48.95 (C-1′), 80.07 (C-2′), 36.86 (C-3′), 44.98 (C-4′), 28.06 (C-5′), 27.24 (C-6′), 47.85 (C-7′), 19.71 (C-8′), 18.86 (C-9′), 13.53 (C-10′).

2.6. Reducing Capacity Tests

2.6.1. Folin–Ciocalteu Reaction. The total antioxidant activity (TAA) was evaluated using the Folin–Ciocalteu assay, which relies on the reagent's reduction in alkaline conditions, yielding a blue chromophore. In this assay, 100-μL aliquots of suitably diluted PA samples were analyzed in duplicate. These were mixed with 3 mL of 2% sodium carbonate, followed by 100 μL of a 1:1 water-diluted Folin–Ciocalteu reagent. The mixture was incubated for 60 min at room temperature in the dark. Absorbance was measured at 765 nm using a DU 640 spectrophotometer (Beckman, Milan, Italy), with a blank as a reference. A standard curve was prepared using gallic acid solutions ranging from 5 to 100 μg/mL, and results were expressed as mg of gallic acid equivalents (GAE) per gram of PA [49].

2.6.2. Ferric Ion Reducing Antioxidant Power (FRAP) Assay. The FRAP assay was performed with slight adaptations from the protocol established by Attanzio et al. [50]. Briefly, 200 μL of the PA ethanolic extract was mixed with an equal volume of 0.2 M phosphate buffer (pH 6.6), followed by the addition of 200 μL of a 1% potassium ferricyanide solution. The mixture was incubated at 50°C for 20 min. After incubation, 200 μL of 10% trichloroacetic acid was added, and the sample was vortexed thoroughly. The mixture was then centrifuged at 1000 × g for 10 min. From the supernatant, 500 μL were transferred into a fresh tube, combined with 1 mL of double-distilled water and 100 μL of 0.1% ferric chloride solution. The absorbance of this final solution was recorded at 700 nm. Antioxidant capacity was determined using a calibration curve generated with ascorbic acid standards (0–100 μg/mL) and expressed as mg of ascorbic acid equivalents (AAE) per gram of PA.

2.7. Radical Scavenging Assays

2.7.1. ABTS•+ Radical Scavenging Assay. The antiradical activity of PA was assessed using the ABTS (2,2′-azino-bis(3-ethylbenzothiazoline-6-sulfonic acid)) assay, following the procedure described by Attanzio et al. [50]. The ABTS radical cation (ABTS•$^+$) was generated by reacting ABTS with potassium persulfate. PA samples were tested at three different dilutions, each analyzed in duplicate to ensure values fell within the assay's linear response range. A standard curve was constructed using Trolox, a water-soluble analog of vitamin E. Results were expressed as Trolox equivalent antioxidant capacity (TEAC) and reported in μmol Trolox equivalents (TE) per gram of PA.

2.7.2. 2,2-Diphenyl-1-Picrylhydrazyl (DPPH) Radical Scavenging Assay. The antioxidant activity of PA was assessed using the DPPH radical scavenging assay, as previously described by Attanzio et al. [50], with minor adjustments. In brief, 10 μL of appropriately diluted ethanolic PA extract was added to 1 mL of an ethanol solution of DPPH (1×10^{-4} M). The reaction mixture was left to incubate for 30 min at room temperature in the dark. Absorbance was recorded at 515 nm. All samples were tested in duplicate at three concentration levels and selected to ensure measurements within the linear range of the assay. Trolox, a water-soluble vitamin E analog, was used as the standard, and results were reported as TE per gram of PA. Trolox was dissolved in ethanol, and care was taken to keep the final ethanol concentration in the reaction mixture below 0.1%.

2.8. Cell Cultures and Treatments. Human cell lines A-375 (melanoma), HCT-116 (colorectal cancer), and MCF-7 (breast cancer) were obtained from the American Type Culture Collection (ATCC, Rockville, MD, USA), while the 16-HBE bronchial epithelial cells were purchased from Merck (Milan, Italy). All cultures were maintained between Passages 4 and 10. Cells were grown in 75 cm^2 culture flasks using DMEM, enriched with 10% fetal bovine serum (FBS), 1% nonessential amino acids, 10 mM HEPES, and antibiotics (50 U/mL penicillin and 50 μg/mL streptomycin). Cultures were kept in a humidified incubator at 37°C under 5% CO_2, and the culture medium was refreshed every 2 days. For experimental purposes, cells were plated at a density of 5.5×10^4 cells/cm^2 in either 24- or 96-well plates, or in μ-dish 35-mm formats, and allowed to adhere for 24 h. Treatment with PA was carried out at concentrations ranging from 1 to 200 μM, applied for 24–48 h depending on the assay as shown in Figure 1.

2.9. Cell Viability. The cytotoxic potential of PA was assessed in A-375, HCT-116, MCF-7, and 16-HBE cell lines using a standard colorimetric assay based on mitochondrial activity. This method exploits the ability of viable cells to reduce 3-(4,5-dimethylthiazol-2-yl)-2,5-diphenyl tetrazolium bromide (MTT) into insoluble purple formazan crystals via mitochondrial dehydrogenases. Cells were plated in 96-well plates (Corning Costar, Milan, Italy) at a density of 5.5×10^4 cells/cm^2, allowed to adhere overnight, and subsequently treated with PA or left untreated as a control. After 24 h of exposure, the medium was removed and each well received 4 μL of MTT solution (5 mg/mL). Following a 2-h incubation at 37°C, the supernatant was discarded, and the formazan crystals formed were solubilized in 100 μL of DMSO. Absorbance was recorded at 575 nm using a microplate reader (LTek, INNO, Seongnam, Republic of Korea). Cell viability was calculated relative to untreated control cells, set as 100%. The half-maximal inhibitory concentration (IC_{50}) values were determined using a dose–response inhibition curve generated with Prism 9.5.0 software (GraphPad Software Inc., San Diego, CA, USA). The selectivity index (SI) was calculated by dividing the IC_{50} value for the nontumorigenic 16-HBE cells by those obtained for tumor cell lines [51]. All experiments were performed in triplicate and independently repeated four times.

2.10. Flow Cytometry

2.10.1. Measurement of Phosphatidylserine Exposure. To evaluate phosphatidylserine exposure on the external surface of the plasma membrane, apoptotic cell death was assessed via dual staining with annexin V-FITC and propidium iodide (PI), followed by flow cytometry. Tumor cells were seeded in triplicate at a density of 5.5×10^4 cells/cm^2 in 24-well plates and cultured overnight. The next day, the medium was replaced and cells were treated with PA at IC25 and IC50 concentrations. After a 24-h incubation, cells were detached using trypsin, collected, and resuspended at 1.0×10^6 cells/mL in the staining buffer, following the manufacturer's instructions (eBioscience, San Diego, CA, USA). Double staining was carried out as previously reported [52]. Flow cytometric evaluation was performed using the CytoFLEX system B2-R2-V0 (Beckman Coulter, Brea, CA, USA) on at least 10,000 events per sample, and data were analyzed using CytExpert software (Beckman Coulter, Brea, CA, USA).

2.10.2. Cell Cycle Analysis. To analyze the distribution of cells across the cell cycle phases, flow cytometry was employed. Following a 24-h exposure to PA at concentrations corresponding to IC_{25} and IC_{50}, adherent cells were detached by trypsinization and washed with cold phosphate-buffered saline (PBS). Cell suspensions containing 1×10^6 cells were then incubated with PBS supplemented with 20 μg/mL PI and 200 μg/mL RNase A for 30 min at room temperature, protected from light [53]. Immediately after staining, samples were analyzed by flow cytometry, collecting at least 10,000 events per sample. Cell cycle phase percentages (G0–G1, S, and G2–M) were determined by excluding the sub-G0–G1 population to focus the analysis exclusively on viable cells.

2.10.3. Measurement of Mitochondrial Membrane Potential (MMP). The assessment of MMP ($\Delta\Psi m$) was performed using the lipophilic cationic dye 3,3′-dihexyloxacarbocyanine iodide (DiOC6) (Molecular Probes, Inc., Life Technologies Italia, Monza, Italy). DiOC6 selectively accumulates within the mitochondrial matrix, and a decrease in its fluorescence intensity indicates a loss of $\Delta\Psi m$. Following 24 h of treatment with PA at IC25 and IC50 concentrations, cells were incubated with DiOC6 at a concentration of 40 nmol/L for 15 min at 37°C. Afterward, cells were collected by centrifugation, washed, and resuspended in 500 μL of PBS. Flow cytometric analysis was conducted on samples containing at least 10,000 cells [54].

2.10.4. Measurement of Intracellular ROS. Intracellular ROS levels were measured by monitoring fluorescence changes following the oxidation of 2′,7′-dichlorofluorescin diacetate

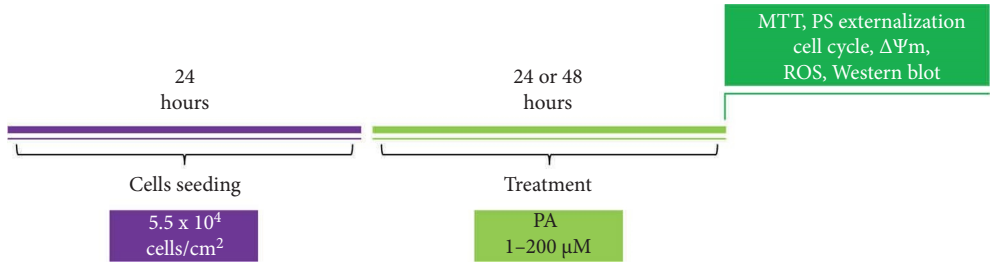

FIGURE 1: Experimental setup. Cells were seeded for 24 h and treated for 24 or 48 h with PA at different concentrations, before studying the parameters indicated.

(DCFDA). After 24 h of PA treatment, DCFDA was added to the culture medium at a final concentration of 1 μM, 30 min prior to the end of the incubation. Cells were then harvested by centrifugation at 25,000 g for 5 min at 4°C, washed, resuspended in PBS, and immediately analyzed by flow cytometry [55]. A minimum of 10,000 events per sample were acquired during the analysis.

2.11. ROS Detection With Fluorescence Microscopy. A375 cells (5.5×10^4 cells/cm^2) were seeded onto μ-dish 35-mm high glass bottom (#1.5H, Ibidi GmbH, Gräfelfing, Germany), which had been precoated with 1.5 mL of poly-L-lysine (100 μg/mL, Merck) for 1 h. After 24 h of adhesion, cells were treated with PA at IC25 and IC50 concentrations for 24 h. Subsequently, cells were washed with PBS and stained with 10 μM DCFDA for 30 min. After a final wash with PBS, fluorescence images were acquired using a Nikon Ts2R fluorescence microscope equipped with a 40x objective and a 23.9-megapixel Digital Sight 10 camera (Nikon Europe B.V., Stroombaan, the Netherlands).

2.12. Western Blot Analysis. After 24 h of treatment, approximately 6×10^6 cells were washed twice with PBS and resuspended in 250 μL of lysis buffer containing 20 mM tris-HCl (pH 7.6), 100 mM NaCl, 10 mM $MgCl_2$, 2 mM PMSF, 0.5 mM DTT, 2 mg/mL lysozyme, and a protease inhibitor cocktail (Roche Applied Science, Indianapolis, IN, 11836170001). Cell disruption was achieved by sonication on ice for 60 s using a Labsonic LBS1-10 device (Falc Instruments srl, Treviglio, Italy). The lysate was then centrifuged at 25,000 g for 1 h at 4°C to separate cellular debris. The supernatant containing the total protein fraction was collected, and protein concentration was determined using the Bradford assay (Bio-Rad, Hercules, CA, USA). Samples were diluted accordingly to load 50 μg of protein per lane on 7.5/10% SDS-PAGE gels. Proteins were resolved by molecular weight and transferred onto nitrocellulose membranes (Cytiva Amersham™ Protran™, Marlborough, MS, USA) through electroblotting. Membranes were blocked with 5% skim milk for 1 h at room temperature to prevent non-specific binding, then incubated overnight at 4°C with primary antibodies against Bcl-2 (sc-7382), BAX (sc-20067), cytochrome c (sc-13156), p53 (sc-397), p21Waf1/Cip1, and actin (sc-8432) from Santa Cruz Biotechnology (SCBT, Dallas, TX, USA). Following two washes with Tween tris-buffered saline (TTBS), membranes were incubated for 1 h at room temperature with horseradish peroxidase–conjugated secondary antibodies (goat anti-mouse or goat anti-rabbit; Merck KGaA, Darmstadt, Germany) diluted 1:2000. Excess secondary antibodies were removed by washing membranes five times with TTBS. Protein detection was performed by chemiluminescence using Amersham ECL reagents (RPN2106, Cytiva Europe GmbH, Freiburg, Germany) [56]. Chemiluminescent signals were captured with a C-Digit Blot Scanner (LI-COR, Lincoln, NE, USA) and quantified using LI-COR Image Studio 4.0 software. Densitometric values were normalized to actin levels, and representative blots were chosen for figure presentation (Figure S7).

2.13. Statistical Analysis. Data are expressed as mean ± standard deviation (SD) from independent experiments, each carried out in triplicate. Statistical differences were evaluated by one-way analysis of variance (ANOVA), followed by Tukey's post hoc test for multiple comparisons, using Prism 9.5.0 software (GraphPad Software Inc., San Diego, CA, USA). A p value less than 0.05 was considered statistically significant throughout the analyses.

3. Results

3.1. Spectroscopical Characterization of PA. To the isolated compound (Figure 2), obtained as an amorphous yellowish powder, the molecular formula $C_{19}H_{24}O_3$ [m/z 323.1638 (M + Na)+ calcd. for $C_{19}H_{24}NaO_3$, 323.1628 Da] was assigned by the HPLC-ESI/MS analysis (Figure S1). The mass spectrum of PA showed a base peak at m/z 137.1337. The IR spectrum presented an intense absorption at 3411 and 1665 cm^{-1}. The presence of a α, β-conjugated ester group was confirmed by a clear signal at 168.09 ppm in the ^{13}C-NMR spectrum (Figure 2). Subsequently, the other peaks identified in the carbon and proton (Figure S2) spectra and 2D-NMR experiments, such as HMBC (Figure S3), HSQC (Fig.ure S4), COSY (Figure S5), and NOESY (Figure S6), clarified the presence of a 10-carbon bicyclic unit ((−)-borneol) linked to the ester moiety. The monoterpene part was, in turn, characterized by three methyl groups at 19.71 (C-8′), 18.86 (C-9′), and 13.53 (C-10′) ppm, three methylene units at 36.86 (C-3′), 28.06 (C-5′), and 27.24 (C-6′) ppm, two methines at 80.07 (C-2′), and 44.98 (C-4′), and two quaternary carbons on C-1′ and C-7′. The coupling constant (J) between protons H_2 and H_3 confirmed, not only

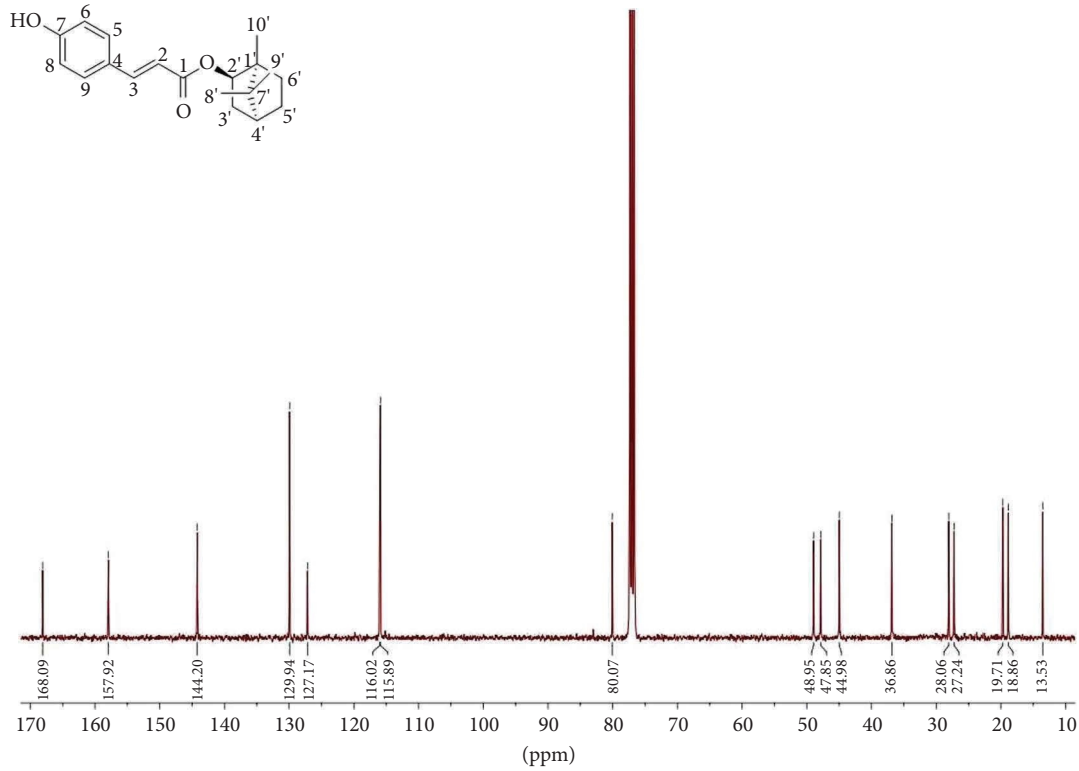

Figure 2: Chemical structure, nomenclature, and ^{13}C-NMR spectrum of PA.

the presence of a double bond but also a clear *cis*-type isomerism ($\delta_H = 6.33–7.63$, each for a proton, d, $J = 15.8$ Hz). The spectroscopic and optical results are in perfect agreement with the literature data [29, 36]. To this compound was then assigned the structure of (−)-bornyl *p*-coumarate, also commonly called PA.

As already mentioned in the introductory part, PA was isolated from plants belonging to different families such as Asteraceae [41, 42], Cistaceae [29], Magnoliaceae [34, 35], and Piperaceae [38], but it has never been isolated in the *Ferulago* genus and in plants of the Apiaceae family.

3.2. Reducing Capacity of PA. The isolated PA exhibited a TAA of 71.05 ± 0.22 mg GAE per gram of compound, as determined by the Folin–Ciocalteu assay (Table 1), indicating a substantial antioxidant potential. Consistently, the FRAP assay revealed a reducing capacity of 6.87 ± 0.41 mg AAE per gram of compound (Table 1). Together, these findings suggest that PA possesses notable antioxidant properties, although the magnitude of activity varies depending on the assay employed.

3.3. Radical Scavenging Activity of PA. The antiradical potential of PA was evaluated through its capacity to neutralize DPPH• and ABTS•+ radicals. In this study, PA demonstrated a DPPH• radical quenching capacity equivalent to 7.72 ± 0.42 μmol Trolox per gram of compound (Table 1). This result suggests that PA has a moderate ability to donate electrons or hydrogen atoms to neutralize free radicals, thereby contributing to its overall antioxidant profile. In addition to the DPPH• assay, the ABTS•+ decolorization assay was employed to further assess PA's antioxidant properties. In these experiments, PA exhibited a quenching ability of 11.38 ± 0.07 μmol Trolox per gram of compound (Table 1), indicating a stronger antiradical activity compared to the DPPH• assay.

Table 1: Reducing capacity and radical scavenger activity of PA.

TAA[a]	FRAP	DPPH•	ABTS•+
mg GAE[b]/g	mg AAE[c]/g	μmolTE[d]/g	
71.05 ± 0.22	6.87 ± 0.41	7.72 ± 0.42	11.38 ± 0.07

Note: Values are the mean ± SD of four determinations carried in triplicate.
[a]TAA, total antioxidant activity.
[b]GAE, gallic acid equivalent.
[c]AAE, ascorbic acid equivalent.
[d]TE, Trolox equivalent.

3.4. Cytotoxic Activity and SI of PA. The antiproliferative activity of PA against various human cancer cell lines was evaluated using the MTT assay, a standard method for measuring cell viability and proliferation [57]. In this study, PA was tested in a concentration range between 1 and 200 μM, with exposure times of 24 and 48 h. The cancer cell lines tested included A-375, HCT-116, and MCF-7. Furthermore, the cytotoxic effect of PA was evaluated on normal 16-HBE cells to determine the SI in comparison to tumor cells (Figure 3).

The IC_{50} values were determined for each cell line. At 24 h, the IC_{50} values were 12.4 ± 0.38 for A-375, 42.54 ± 1.56 for HCT-116, and 54.51 ± 2.43 μM for MCF-7, respectively. After 48 h, the IC_{50} values decreased to 6.08 ± 0.26 for A-375,

28.68 ± 1.26 for HCT-116, and 23.72 ± 1.76 μM for MCF-7, indicating a time-dependent increase in PA's cytotoxicity (Table 2). These results demonstrate that PA exhibits significant cytotoxic activity across all tested cancer cell lines, with the A-375 cells being the most sensitive. In contrast, the viability of noncancerous 16-HBE cells was much less affected by PA, with IC_{50} values of 140.7 ± 17.23 and 104.7 ± 7.98 μM at 24 and 48 h, respectively (Table 2).

This indicates that PA has a higher selectivity for cancer cells over noncancerous cells, which is a desirable characteristic in anticancer drug development.

Selective cytotoxicity is a crucial criterion for the development of effective anticancer agents [59]. To evaluate the selectivity of PA, its cytotoxic effects on the cancer cell lines A-375, HCT-116, and MCF-7 were compared to its effects on 16-HBE cells. The SIs of PA were 11.34, 2.58, and 3.31 at 24 h, and 23.14, 5.93, and 4.90 at 48 h for the A-375, HCT-116, and MCF-7 cell lines, respectively. These findings are particularly noteworthy for the A-375 cell line, where the SI values exceed 10, indicating strong selectivity and antiproliferative activity in vitro [58, 59].

The high SI for A-375 cells suggests that PA is especially effective against melanoma cells, with minimal impact on noncancerous cells (Table 3).

3.5. PA Induces a ROS-Dependent Mitochondrial Apoptotic Pathway in A-375 Cells. To investigate whether the antiproliferative effect of PA was driven by apoptosis or necrosis, flow cytometry analysis was performed on A-375 cells double-stained with annexin V-FITC and PI. The concentrations of PA used in this study were selected based on its IC_{50} value at 24 h for the A-375 cell line. Specifically, IC_{50} at 12.4 μM and IC_{25} at 6.2 μM were tested (Table 2). The results, presented in Figure 4, demonstrate that neither concentration of PA induced significant necrotic effects in A-375 cells, as indicated by the low percentage of necrotic cells—1.2% and 1.5% for $IC_{25,}$ and IC_{50}, respectively—compared to 1.4% in the control cells.

In contrast, a clear concentration-dependent shift from viable to apoptotic cells was observed, especially toward early apoptosis (Figure 4). The proportion of annexin V-FITC positive cells, indicative of apoptosis, increased with PA concentration, reaching 16.8 ± 0.9% and 22.8 ± 1.7% for IC_{25} and IC_{50}, respectively, compared to 5.8 ± 0.4% in the control cells ($p < 0.001$, Figure 4).

These findings suggest that PA predominantly induces apoptosis rather than necrosis in A-375 cells, with a stronger apoptotic response observed at higher concentrations.

In many cellular systems, the depolarization of MMP is indicative of mitochondrial dysfunction, often leading to the loss of the inner MMP (ΔΨm) [60]. This loss is a critical factor in the release of proapoptotic factors from the mitochondria and is considered an early event in the apoptotic process [61].

To assess the impact of PA on mitochondrial function, flow cytometry was employed to measure ΔΨm using DiOC6. The results demonstrated a concentration-dependent increase in mitochondrial dysfunction following 24 h of treatment with PA in A-375 cells. Specifically, there was a 3.5-fold increase in mitochondrial depolarization at a concentration of PA equivalent to IC_{25} and a 5.3-fold increase at the IC_{50} concentration, compared to untreated control cells ($p < 0.001$, Figure 5).

These findings suggest that PA induces significant mitochondrial dysfunction, which is likely to contribute to the observed apoptotic effects in A-375 cells.

Since the alteration of cellular redox homeostasis is closely associated with mitochondrial dysfunction and induction of apoptosis in various cell types [62–66], the production of intracellular ROS induced by PA was investigated. As shown in Figures 6(a) and 6(b), the treatment with PA led to a significant, concentration-dependent increase in ROS levels in A-375 cells, as measured by flow cytometry using the fluorescent dye DCFDA. Specifically, PA treatment resulted in a 4.2-fold increase in ROS production at a concentration corresponding to IC_{25} and a 6.1-fold increase at the IC_{50}, compared to untreated control cells ($p < 0.001$).

Fluorescence microscopy visualization of the cells confirmed an increase in DCFDA-associated fluorescence intensity caused by PA treatment in a concentration-dependent manner (Figure 6(c)). Additionally, a proportional decrease in the number of observed cells is noted as the concentration of PA increases. This substantial rise in ROS production is strongly correlated with the loss of mitochondrial integrity, which is a critical event that can precipitate irreversible cellular damage and trigger apoptosis [67, 68].

3.6. PA Induces Cell Cycle Arrest at the G1-S Transition in A-375 Cells. Evaluation of cell cycle phase distribution was performed by flow cytometry, analyzing DNA content via PI staining after incubating A-375 cells with PA for 24 h. PA treatment induced an accumulation of A-375 cells at the G1-S transition and a reduction in the G2-M phase. Specifically, cells treated with PA at concentrations corresponding to IC_{25} and IC_{50} showed a modest but statistically significant increase in the G0-G1 phase, with 63.9 ± 3.8% and 65.5 ± 4.6% of cells in this phase, respectively, compared to 57.3 ± 3.2% in control cells ($p < 0.05$ and $p < 0.01$, Figure 7). Concurrently, PA treatment was associated with an increase in the percentage of cells in the S phase. Notably, the S-phase population was 15.3 ± 0.8% and 20.1 ± 1.6% for IC_{25} and IC_{50} treatments, respectively, compared to 12.5 ± 0.5% in control cells ($p < 0.05$ and $p < 0.001$, Figure 7). Additional treatment with PA at concentrations IC_{25} and IC_{50} showed 20.9 ± 1.1% and 15.1 ± 0.6% of cells in the G2-M phase, respectively, compared to 29.9 ± 1.6% in untreated control cells ($p < 0.001$, Figure 7).

This arrest of cell cycle progression, with the accumulation of cells at the G1-S phase, contributes to the overall antiproliferative effects of PA.

3.7. PA Dysregulates Apoptosis-Related Protein Levels. Mitochondrial dysfunction is a critical determinant in the regulation of the intrinsic apoptosis pathway [69]. To gain deeper insights into this mechanism, we employed Western

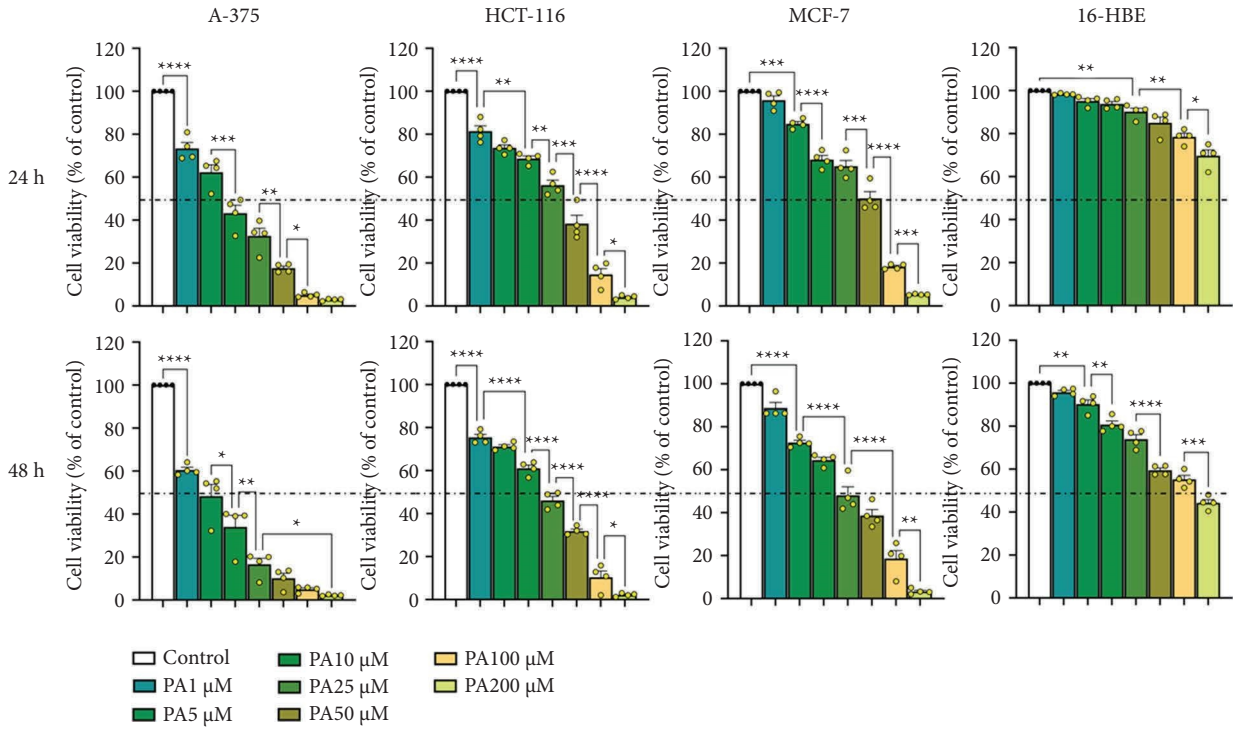

FIGURE 3: Antiproliferative activity of PA on A-375, HCT-116, MCF-7, and 16-HBE cells. Cell viability was assessed after 24 or 48 h of treatment by MTT assay. $^{*}p < 0.05$, $^{**}p < 0.01$, $^{***}p < 0.005$, and $^{****}p < 0.001$. Values are the mean ± SD of four separate experiments conducted in triplicates.

TABLE 2: IC_{50} of PA against A-375, HCT-116, MCF-7, and 16-HBE cell lines.

Treatment time	PA IC_{50} (μM)			
	A-375	HCT-116	MCF-7	16-HBE
24 h	12.4 ± 0.38	42.54 ± 1.56	54.51 ± 2.43	140.7 ± 17.23
48 h	6.08 ± 0.26	28.68 ± 1.26	23.72 ± 1.76	104.0 ± 7.98

Note: Values were calculated by plotting the percentage viability versus concentration on a logarithmic graph. Values are the mean ± SD of four separate experiments conducted in triplicates.

TABLE 3: SI of PA on A-375, HCT-116, and MCF-7 cell lines.

Treatment time	Selectivity index		
	A-375	MCF-7	HCT-116
24 h	11.34	2.58	3.31
48 h	23.14	5.93	4.90

blot analysis to investigate the involvement of key apoptotic markers—BAX, Bcl-2, and cytochrome c—based on the cytofluorimetric data previously obtained. Given the pronounced effects observed in the cytofluorimetric assays, A-375 cells were treated for 24 h in the presence or absence of PA at its IC_{50} concentration. In particular, Western blot analysis showed that PA treatment significantly reduced Bcl-2 protein levels by 47% compared to untreated controls ($p < 0.01$, Figure 8). Conversely, BAX and cytochrome *c* protein levels were markedly elevated following PA exposure, with increases of 33.6% and 55.6%, respectively ($p < 0.01$ and $p < 0.005$, Figure 8). Notably, the expression of BAX and Bcl-2 is regulated by the tumor suppressor protein p53, which is a key mediator of apoptosis [70]. These findings indicate that PA treatment significantly upregulated p53 protein levels in A-375 cells, showing a substantial 328% increase ($p < 0.001$, Figure 8). Among the downstream effectors of p53, $p21^{Waf1/Cip1}$ is a crucial regulator of cell cycle arrest and apoptosis [71]. The treatment with PA resulted in a significant upregulation of $p21^{Waf1/Cip1}$ protein levels, with a 67% increase observed in comparison to untreated cells ($p < 0.001$, Figure 8).

4. Discussion

The search for natural antioxidants for applications in nutrition, cosmetics, and pharmacology has emerged as a major scientific and industrial challenge over the past 30 years [72]. Between the natural bioactive compounds, terpenoids and their derivatives have been recognized for their biological effects, including antioxidant and antiproliferative properties [73–75]. Many studies have also examined the in vitro effects of terpenoids on various human melanoma cell lines, including A-375 cells [76–80]. In this study, PA demonstrated significant TAA. The Folin–Ciocalteu assay indicated high TAA, while the FRAP assay confirmed PA's notable ferric ion reduction capability. The difference between these results suggests that PA is effective in general antioxidant activity but somewhat less potent as a reducing agent. This underscores the need for multiple assays to comprehensively assess a compound's antioxidant potential.

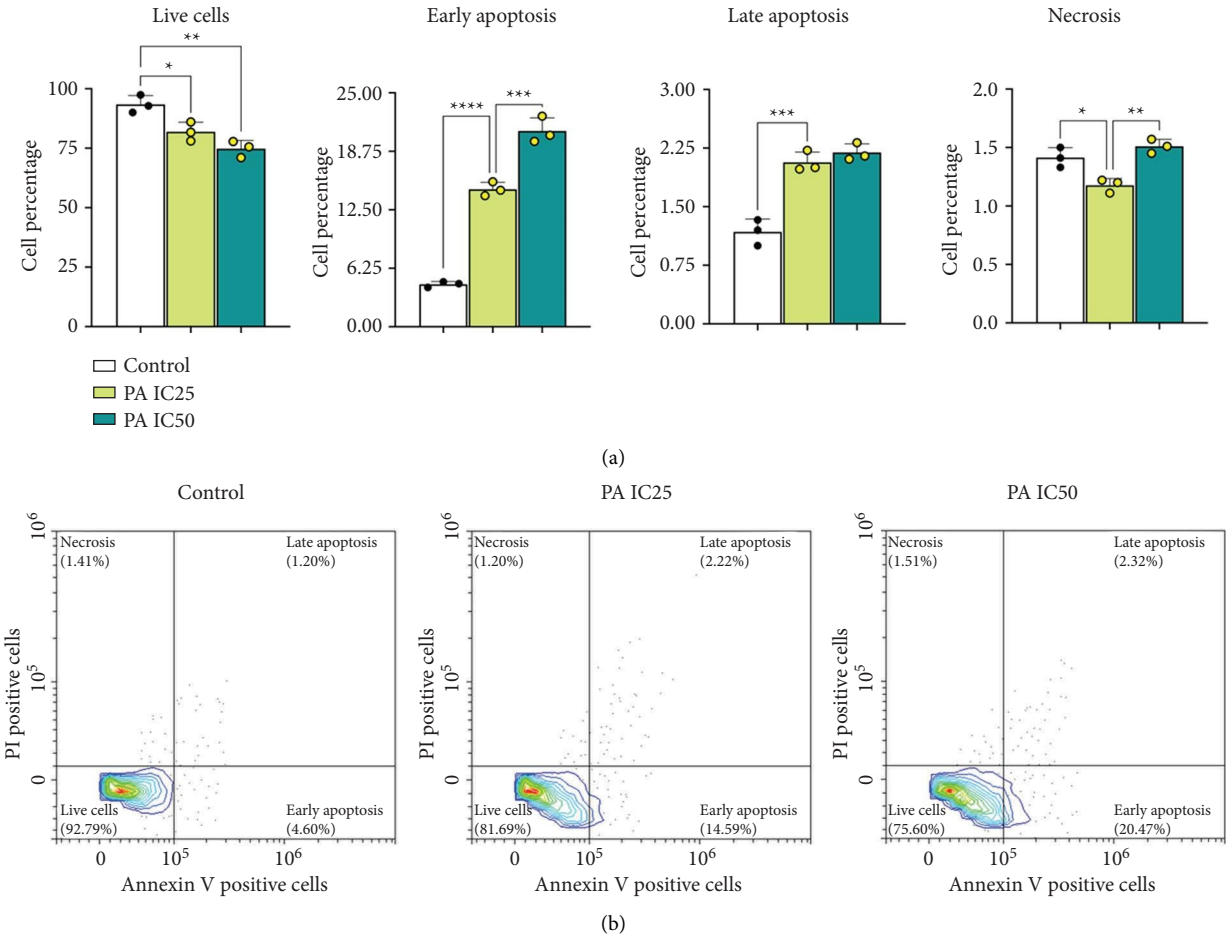

FIGURE 4: Effect of PA on the externalization of PS in A-375 cells. Cells were treated for 24 h as described in the Methods section. Percentage of AnnexinV-FITC/PI double stained A-375 cells were determined by flow cytometer and compared to untreated cells (control). (a) Mean values ± SD of three separate experiments in triplicate. $^{*}p < 0.05$, $^{**}p < 0.01$, $^{***}p < 0.005$, and $^{****}p < 0.001$ (one-way ANOVA associated with Tukey's post hoc test). (b) Representative flow cytometric images: live cells (AnnexinV−/PI−); early apoptotic cells (AnnexinV+/PI−); late apoptotic cells (AnnexinV+/PI+); necrotic cells (AnnexinV−/PI+).

PA also exhibited considerable radical scavenging activity, particularly evident in the ABTS•+ assay. The differences observed between the DPPH• and ABTS•+ assays likely arise from the distinct chemical environments and mechanisms of each assay. The DPPH• assay primarily evaluates hydrogen atom transfer (HAT), while the ABTS•+ assay accommodates single electron transfer (SET) reactions [81]. This indicates that PA may be more effective at scavenging radicals via SET mechanisms, which are relevant under physiological conditions where both HAT and SET pathways contribute to antioxidant defense. Overall, PA's efficacy as an antiradical agent is highlighted by its ability to neutralize various free radicals through multiple mechanisms (Table 1) and is comparable to other terpenoids such as α-terpinene, ocimene, and pulegone [82]. This antiradical activity is a crucial component of PA's broader antioxidant profile, suggesting potential therapeutic applications. Additionally, this study offers, for the first time, significant insights into PA's anti-proliferative and cytotoxic effects on human cancer cell lines, with a focus on melanoma. The IC50 values indicate that PA's cytotoxicity is time-dependent in A-375 cells, with IC50 values of 12.4 μM at 24 h and 6.08 μM at 48 h. In contrast, higher IC50 values for HCT-116 and MCF-7 cells suggest these cells are less sensitive to PA. A key finding is PA's selectivity for cancer cells over noncancerous cells. The viability of 16-HBE cells was less affected by PA, with IC50 values significantly higher than those in cancer cells. SI's values were remarkably high for A-375 cells, exceeding 10 at both 24 and 48 h, indicating strong selectivity. This suggests PA's potential as a therapeutic agent against melanoma with minimal impact on noncancerous cells. To further investigate the antiproliferative effect of PA, we examined whether it induces cell death via apoptosis or necrosis. Flow cytometry analysis revealed that PA predominantly induces apoptosis rather than necrosis in A-375 cells. The proportion of apoptotic cells increased in a concentration-dependent manner, with a more pronounced apoptotic response at higher PA concentrations. Apoptosis, being a regulated process of cell death, is generally associated with better therapeutic outcomes compared to necrosis, which can cause inflammation and tissue damage. Further investigation into PA-induced apoptosis mechanisms revealed significant mitochondrial dysfunction in A-375 cells. A concentration-dependent depolarization of mitochondrial

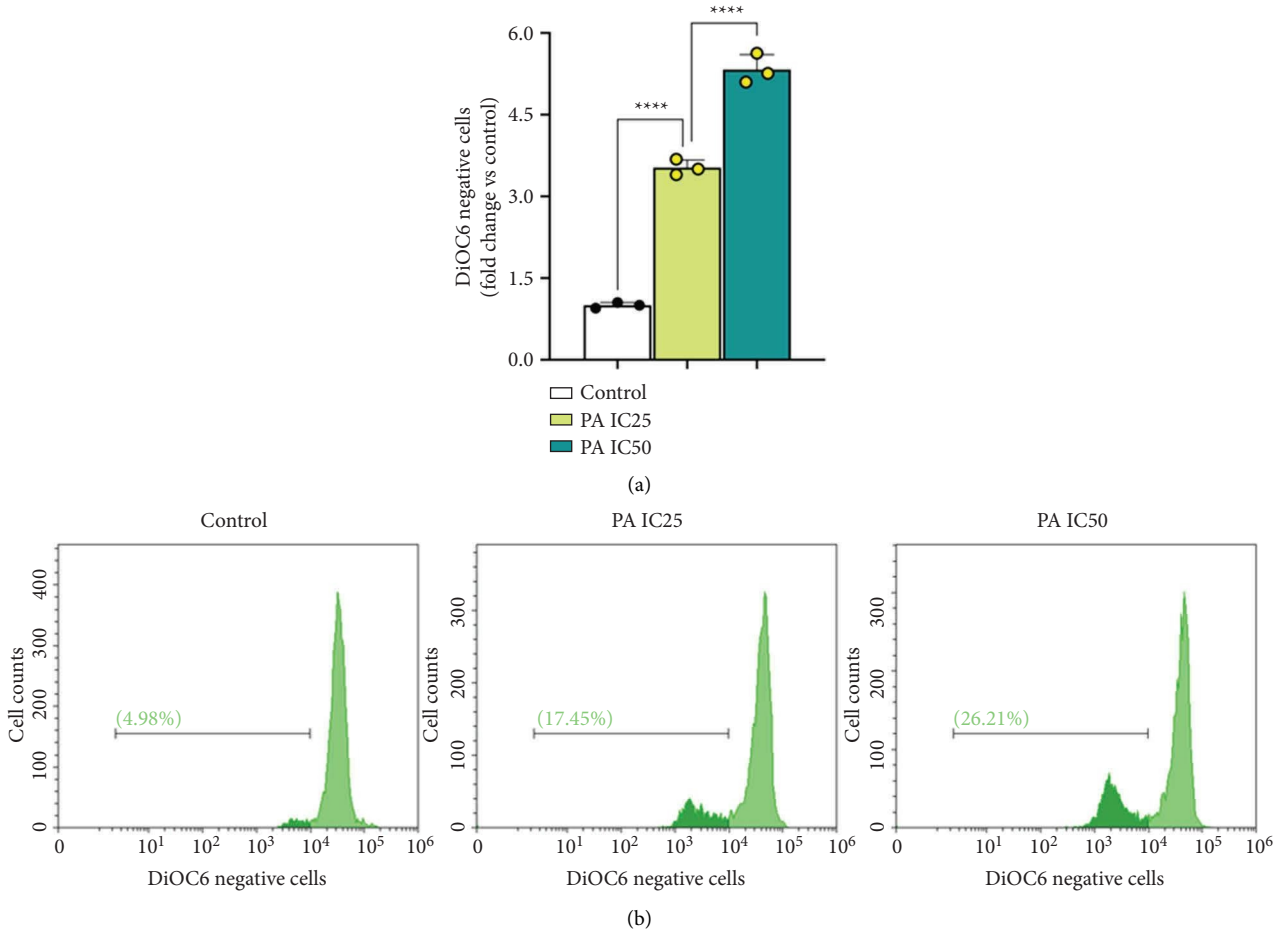

Figure 5: Depolarization of mitochondrial membrane potentially induced by PA on A-375 cells. Cells were treated for 24 h as reported in the Methods section. Then, the percentages of DiOC6 negative-A375 cells were determined by a flow cytometer and compared to untreated cells (control). (a) Mean values ± SD of three separate experiments in triplicate. $^{****}p < 0.001$ (one-way ANOVA associated with Tukey's post hoc test). (b) Representative flow cytometric images.

membrane, a critical event in apoptosis initiation, was observed following PA treatment. The involvement of the intrinsic apoptotic pathway mediated by mitochondrial damage has been highlighted as a feature of other natural compounds by various authors over the last decades (83-85). The loss of MMP is crucial for the release of pro-apoptotic factors from mitochondria, indicating that mitochondrial dysfunction plays a central role in PA-induced apoptosis. Additionally, PA treatment led to a substantial increase in intracellular ROS levels in A-375 cells, which strongly correlates with mitochondrial dysfunction. This result is also in line with recent studies demonstrating that terpenoids such as thymoquinone and thymol exhibit a ROS-dependent anti-proliferative effect (86, 87). As is well known, ROS mediate various cellular processes, including apoptosis, suggesting that oxidative stress is a key component of PA's cytotoxic mechanism (63). Although seemingly paradoxical, many natural compounds exhibit a well-characterized dual behavior, acting as antioxidants under physiological conditions and as pro-oxidants in stressed or transformed cells. At low concentrations, they typically reduce ROS levels and activate cytoprotective pathways such as Nrf2, whereas in cancer cells or at higher doses, they can elevate ROS beyond the cellular threshold, triggering apoptosis or ferroptosis. This selective pro-oxidant cytotoxicity offers a promising therapeutic strategy to target malignant cells while sparing healthy tissue (88-90). Examples include curcumin, which acts as an Nrf2 activator and NF-κB inhibitor in normal cells but induces ROS-mediated mitochondrial apoptosis in tumor cells via glutathione peroxidase inhibition (91, 92). Resveratrol similarly protects normal cells but promotes apoptosis in cancer cells by impairing mitochondrial function and increasing ROS [93, 94]. Celastrol, known for its anti-inflammatory effects, also induces ROS accumulation and apoptosis selectively in tumor contexts (95, 96). This redox-dependent behavior highlights the potential of these compounds as context-specific anticancer agents. PA also affected the distribution of cells across different cell cycle phases. In line with other terpenoids in alternative in vitro models (97, 98), the increased cell population in S-phase may indicate DNA replication stress, possibly due to PA-induced cellular damage or interference with DNA synthesis. This stress can lead to cell cycle arrest and potentially trigger apoptotic pathways if the damage is irreparable. The modest increase in the G0-G1 phase suggests that PA treatment may influence early cell cycle phases. The accumulation of cells in G0-G1 could reflect checkpoint

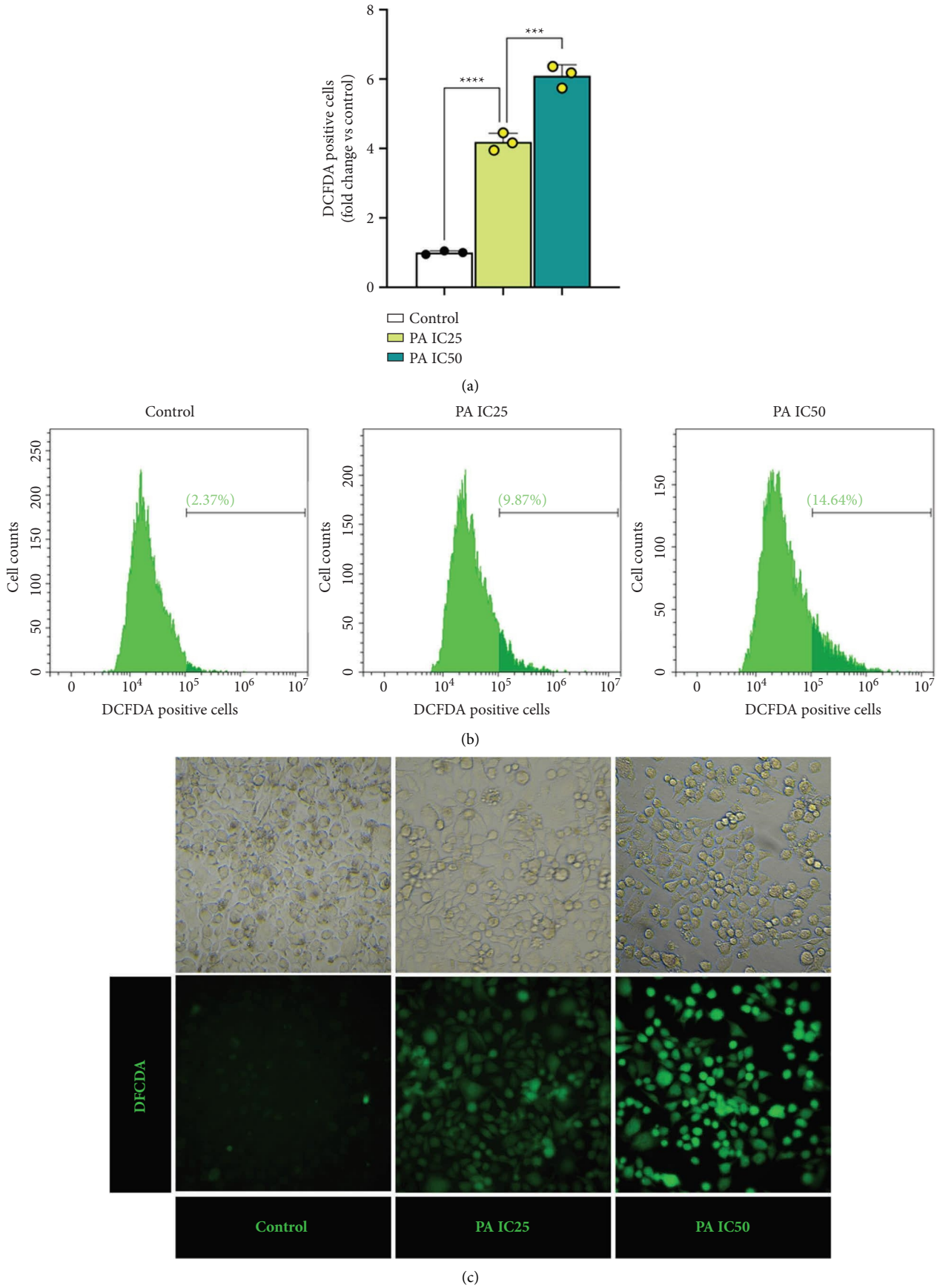

FIGURE 6: Effect of PA on ROS production in A-375 cells. ROS levels were evaluated using flow cytometry and fluorescence microscopy after 24 h of treatment by staining of the cells with DCFDA as reported in Methods. Data are compared to untreated cells (control). (a) Mean values ± SD of three separate experiments in triplicate. $^{***}p < 0.005$ and $^{****}p < 0.001$ (one-way ANOVA associated with Tukey's post hoc test). (b) Representative flow cytometric images. (c) Representative fluorescence microscopy images.

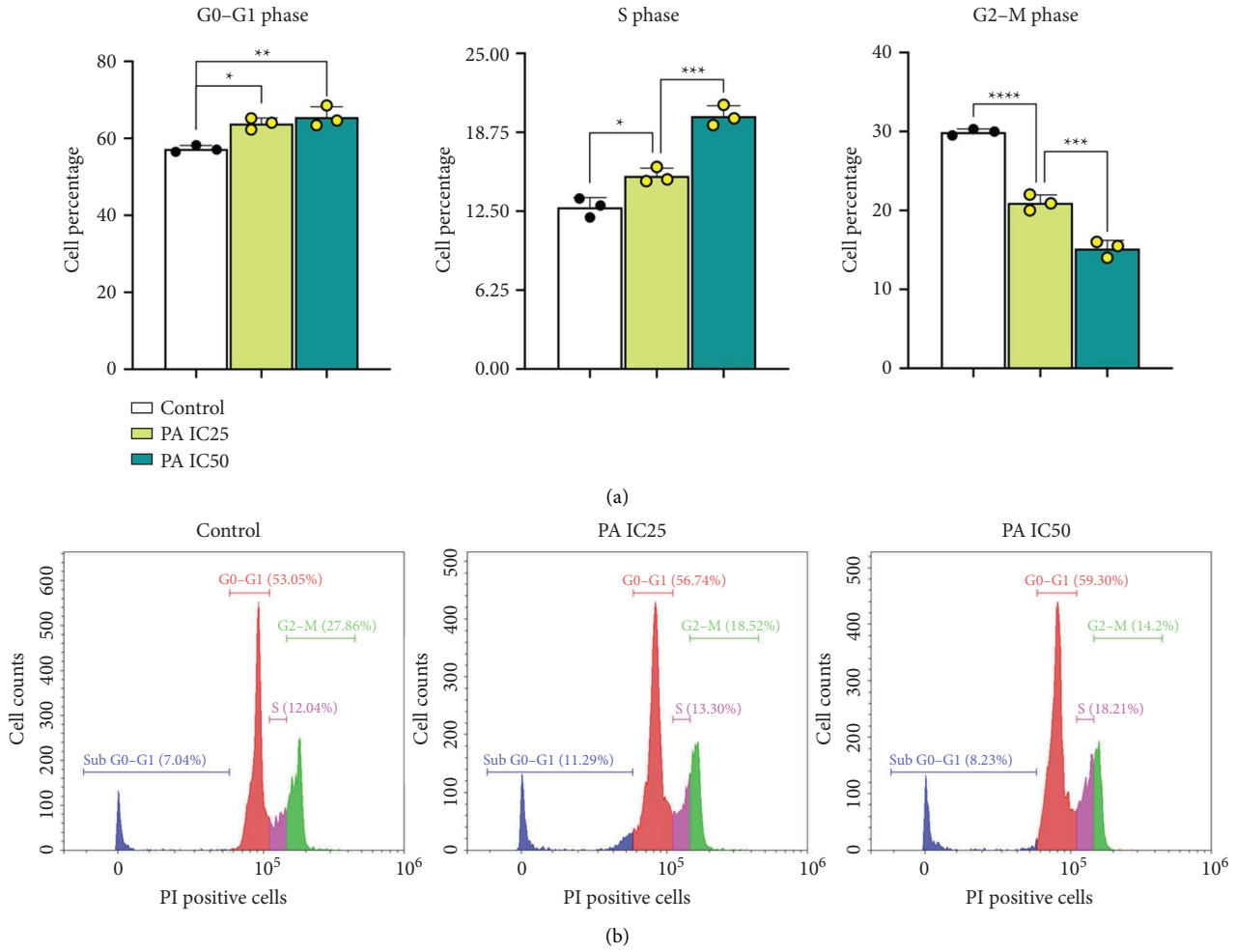

Figure 7: Effect of PA on the distribution of cell cycle phases in A-375 cells. Cells were treated for 24 h as described in the Methods section. Then, samples were submitted to flow cytometry analysis after PI staining and cell distribution compared to untreated cells (control). (a) Each bar shows the percentage of viable cells in the different phases. $^{*}p < 0.05$, $^{**}p < 0.01$, $^{***}p < 0.005$, and $^{****}p < 0.001$ (one-way ANOVA associated with Tukey's post hoc test). (b) Representative flow cytometric images.

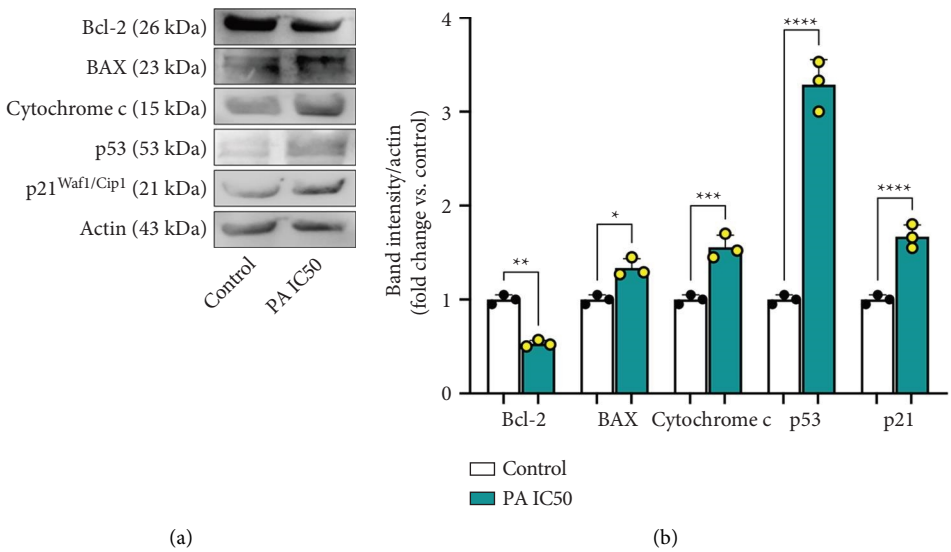

Figure 8: Effect of PA on protein levels of apoptosis and cell cycle–related proteins in A-375 cells. Cells were treated for 24 h as described in Methods section. (a) Representative images of analyzed proteins. (b) Densitometric analysis of BAX, Bcl-2, cytochrome c, p53, and $p21^{Waf1/Cip1}$ normalized for actin. Values are the means ± SD of bands' densitometry of three independent experiments with comparable results. $^{*}p < 0.05$, $^{**}p < 0.01$, $^{***}p < 0.005$, and $^{****}p < 0.001$ (one-way ANOVA associated with Tukey's post hoc test).

activation in response to PA-induced stress or a compensatory mechanism addressing disruptions in later cell cycle phases (99). In summary, PA induces significant changes in the distribution of cells across cell cycle phases that align with its apoptotic effects. These results underscore the complex interactions between PA and cellular processes, including cell cycle regulation and apoptosis. Mitochondrial dysfunction plays a central role in regulating the intrinsic apoptotic pathway, primarily driven by an imbalance in the ratio of pro-apoptotic BAX and anti-apoptotic Bcl-2 proteins (100). This dysregulation leads to mitochondrial outer membrane permeabilization, triggering the release of cytochrome c and subsequent assembly of apoptosome (101). Western blot analysis of key apoptotic markers–BAX, Bcl-2, and cytochrome c–revealed that PA treatment led to a significant decrease in Bcl-2 protein levels and a notable increase in BAX and cytochrome c protein levels. The expression of these markers is influenced by the tumor suppressor protein p53, which regulates apoptosis (102,103). PA treatment caused a substantial increase in the amount p53 and its downstream target p21Waf1/Cip1, a critical regulator of cell cycle arrest and apoptosis. These findings underscore the role of PA in modulating key components of the intrinsic apoptotic pathway through the activation of p53 and its downstream targets. The substantial alterations in the levels of BAX, Bcl-2, cytochrome c, and p21Waf1/Cip1 suggest that PA induces apoptosis primarily via the mitochondrial pathway, thereby highlighting its potential as a therapeutic agent in the treatment of skin disease as melanoma.

5. Conclusion

Terpenoids represent a class of compounds with significant pharmacological importance due to their diverse bioactivities and therapeutic potential. Despite their promising applications, there are several challenges associated with terpenes that require further investigation, including issues related to toxicity, safety, bioavailability, and their mechanisms of action. Future research should focus on elucidating whether PA can effectively combat oxidative stress and inflammation in biological systems, both in vitro and in vivo. Understanding PA's role in mitigating oxidative stress and preventing related diseases could provide critical insights into its potential as a natural antioxidant source.

In summary, the study highlights that PA exhibits potent antiproliferative and proapoptotic effects against human cancer cell lines, particularly A-375 melanoma cells. PA's high selectivity for cancer cells over noncancerous cells, coupled with its ability to induce apoptosis through mitochondrial dysfunction and ROS generation, underscores its potential as a therapeutic agent. These findings suggest that further investigation is warranted, including the use of advanced analytical tools such as artificial intelligence (AI), to explore the specific pathways through which PA induces apoptosis.

Nomenclature

AAE	ascorbic acid equivalents
ABTS	2,2′-azino-bis(3-etilbenzotiazolin-6-sulfonic acid)
PA	Pressafonin-A
DCFDA	2′,7′-dichlorofluorescin diacetate
DiOC6	3,3′-dihexyloxacarbocyanine iodide
DMEM	Dulbecco's modified Eagle's medium
DMSO	dimethyl sulfoxide
DPPH	2,2-Diphenyl-1-picrylhydrazyl
FBS	fetal bovine serum
FRAP	ferric reducing antioxidant power
GAE	gallic acid equivalents
HPLC-ESI/MS^n	High-performance liquid chromatography/electrospray ionization tandem mass spectrometry
MTT	3-(4,5-dimethylthiazol-2-yl)-2,5-diphenyltetrazolium bromide
NMR	Nuclear magnetic resonance
PBS	phosphate-buffered saline
PI	propidium iodide
ROS	reactive oxygen species
SD	standard deviation
SI	selectivity index
TAA	total antioxidant activity
TE	Trolox equivalents
TEAC	Trolox equivalents antioxidant capacity
TLC	Thin layer chromatography
TMS	tetramethylsilane
TTBS	Tween tris-buffered saline
ΔΨm	change in mitochondrial membrane potential

Data Availability Statement

The data used to support the findings of this study are included in the Supporting Information. Further inquiries can be directed to the corresponding authors upon reasonable request.

Conflicts of Interest

The authors declare no conflicts of interest.

Author Contributions

Conceptualization: Natale Badalamenti; data curation: Ilenia Concetta Giardina, Ignazio Restivo, and Natale Badalamenti; formal analysis: Alessandro Attanzio, Ignazio Restivo, and Natale Badalamenti; funding acquisition: Maurizio Bruno, Natale Badalamenti, and Luisa Tesoriere; investigation: Alessandro Massaro, Ilenia Concetta Giardina, Ignazio Restivo, and Natale Badalamenti; methodology: Alessandro Attanzio, Ignazio Restivo, Maurizio Bruno, and Natale Badalamenti; resources: Alessandro Attanzio, Maurizio Bruno, and Luisa Tesoriere; software: Ignazio Restivo and Natale Badalamenti; supervision: Alessandro Attanzio, Maurizio Bruno, and Luisa Tesoriere; validation: Alessandro Attanzio, Ignazio Restivo, Mario Allegra, Natale Badalamenti, and Luisa Tesoriere; visualization: Ignazio Restivo and Natale Badalamenti; writing – original draft:

Ignazio Restivo and Natale Badalamenti; writing – review and editing: Alessandro Attanzio, Maurizio Bruno, and Luisa Tesoriere.

Funding

This research work was financially supported by the National Biodiversity Future Center S.c.a.r.l., Piazza Marina 61 (c/o Palazzo Steri) Palermo, Italy, C.I. CN00000033, CUP UNIPA B73C22000790001 and European Union - Next Generation EU (PRIN-PNRR), project code P2022CKMPW_002 - CUP B53D23025620001. Dr. Ignazio Restivo was supported by Fondazione Umberto Veronesi.

Acknowledgments

Dr. Ignazio Restivo was supported by Fondazione Umberto Veronesi.

Supporting Information

Additional supporting information can be found online in the Supporting Information section. *(Supporting Information)*

Supplementary material 1 Figure S1: Mass spectrum of pressafonin-A (PA).

Supplementary material 2 Figure S2: 1H-spectrum of pressafonin-A (PA).

Supplementary material 3 Figure S3: HMBC spectrum of pressafonin-A (PA).

Supplementary material 4 Figure S4: HSQC spectrum of pressafonin-A (PA).

Supplementary material 5 Figure S5: COSY spectrum of pressafonin-A (PA).

Supplementary material 6 Figure S6: NOESY spectrum of pressafonin-A (PA).

Supplementary material 7 Figure S7: Complete blot images in Figure 8.

References

[1] POWO, *Plants of the World Online* (2024), https://powo.science.kew.org/results?q=Ferulago.

[2] L. P. Tomkovich and M. G. Pimenov, "Botanico-Geographical Analysis of the Genus *Ferulago*," *W.D.J. Koch. Feddes Reper.* 100, no. 3-4 (1989): 119–129, https://doi.org/10.1002/fedr.4911000305.

[3] L. Peruzzi, G. Domina, F. Bartolucci, et al., "An Inventory of the Names of Vascular Plants Endemic to Italy, Their Loci Classici and Types," *Phytotaxa* 196 (2015): 1–217, https://doi.org/10.11646/phytotaxa.196.1.1.

[4] A. Troia, F. M. Raimondo, G. Castellano, and V. Spadaro, "Morphological, Karyological and Taxonomic Remarks on *Ferulago nodosa* (L.) Boiss. (Apiaceae)," *Plant Biosystems-An International Journal Dealing With all Aspects of Plant Biology* 146, no. 1 (2012): 330–337, https://doi.org/10.1080/11263504.2012.716797.

[5] N. Badalamenti, V. Ilardi, S. Rosselli, and M. Bruno, "The Ethnobotany, Phytochemistry and Biological Properties of Genus *Ferulago*–A Review," *Journal of Ethnopharmacology* 274 (2021): 114050, https://doi.org/10.1016/j.jep.2021.114050.

[6] Y. Shahbazi, "Variation in Chemical Composition of Essential Oil of *Ferulago angulata* Collected From West Parts of Iran," *Pharmaceutical Sciences* 22, no. 1 (2016): 16–21, https://doi.org/10.15171/ps.2016.04.

[7] S. Karakaya, M. Koca, C. S. Kılıc, and M. Coskun, "Antioxidant and Anticholinesterase Activities of *Ferulago syriaca* Boiss. and *F. Isaurica* Peşmen Growing in Turkey," *Medicinal Chemistry Research* 27, no. 7 (2018): 1843–1850, https://doi.org/10.1007/s00044-018-2196-7.

[8] N. Arnold, S. Baydoun, L. Chalak, and T. Raus, "A Contribution to the Flora and Ethnobotanical Knowledge of Mount Hermon, Lebanon," *Flora Mediterranea* 25 (2015): 13–55.

[9] G. Sadeghi, M. Habibian, A. Raei, D. Farhadi, and N. Khateri, "Effects of Dietary Supplementation of *Ferulago angulata* (Schlecht.) Boiss Powder on Growth Performance, Carcass Characteristics, and Gut Microflora and pH in Broiler Chicks," *Comparative Clinical Pathology* 25, no. 2 (2016): 257–263, https://doi.org/10.1007/s00580-015-2175-z.

[10] V. A. Taddeo, F. Epifano, F. Preziuso, et al., "HPLC Analysis and Skin Whitening Effects of Umbelliprenin-Containing Extracts of *Anethum graveolens, Pimpinella anisum*, and *Ferulago campestris*," *Molecules* 24, no. 3 (2019): 501, https://doi.org/10.3390/molecules24030501.

[11] A. Pieroni, R. Sõukand, H. I. M. Amin, H. Zahir, and T. Kukk, "Celebrating Multireligious Co-existence in Central Kurdistan: the Bio-Culturally Diverse Traditional Gathering of Wild Vegetables Among Yazidis, Assyrians, and Muslim Kurds," *Human Ecology (New York, N. Y.)* 46, no. 2 (2018): 217–227, https://doi.org/10.1007/s10745-018-9978-x.

[12] P. Skandamis, E. Tsigarida, and G. J. E. Nychas, "The Effect of Oregano Essential Oil on Survival/Death of *Salmonella typhimurium* in Meat Stored at 5°C Under Aerobic, VP/MAP Conditions," *Food Microbiology* 19, no. 1 (2002): 97–103, https://doi.org/10.1006/fmic.2001.0447.

[13] S. Karakaya, D. Şimşek, H. Özbek, et al., "Antimicrobial Activities of Extracts and Isolated Coumarins From the Roots of Four *Ferulago* Species Growing in Turkey," *Iranian Journal of Pharmaceutical Research* 18, no. 3 (2019): 1516–1529, https://doi.org/10.22037/ijpr.2019.1100718.

[14] M. Moghaddam, L. Mehdizadeh, H. M. Najafgholi, and A. Ghasemi Pirbalouti, "Chemical Composition, Antibacterial and Antifungal Activities of Seed Essential Oil of *Ferulago angulate*," *International Journal of Food Properties* 21 (2018): 158–170.

[15] S. Karakaya, D. Simsek, G. Göger, B. Demirci, and H. Duman, "Comparison of Essential Oils of *Ferulago pachyloba* (Fenzl) Boiss., F. Trachycarpa Boiss. and F. Bracteata Boiss. & Hausskn. Species (Apiaceae) Growing in Turkey and Determination of Their Antimicrobial Activities," *Journal of Essential Oil Bearing Plants* 22 (2019): 200–213.

[16] S. Bagherifar, M. M. Sourestani, M. Zolfaghari, J. Mottaghipisheh, Z. P. Zomborszki, and D. Csupor, "Variation of Chemical Constituents and Antiradical Capacity of Nine *Ferulago angulata* (Schltdl.) Boiss Populations From Iran," *Chemistry and Biodiversity* 16, no. 10 (2019): e1900302, https://doi.org/10.1002/cbdv.201900302.

[17] N. Badalamenti, V. Ilardi, S. Rosselli, et al., "Maggi. *Ferulago nodosa* Subsp. *Geniculata* (Guss.) Troia & Raimondo From Sicily (Italy): Isolation of Essential Oil and Evaluation of its Bioactivity," *Molecules* 25, no. 14 (2020): 3249, https://doi.org/10.3390/molecules25143249.

[18] F. Zare Shahneh, B. Baradaran, M. Orangi, and F. Zamani, "*In Vitro* Cytotoxic Activity of Four Plants Used in Persian Traditional Medicine," *Advanced Pharmaceutical Bulletin* 3, no. 2 (2013): 453–455, https://doi.org/10.5681/apb.2013.074.

[19] F. Z. Shahneh, S. Valiyari, A. Azadmehr, R. Hajiaghaee, A. Bandehagh, and B. Baradaran, "*In Vitro* Cytotoxic and Apoptotic Activity of Four Persian Medicine Plants on Human Leukemia and Lymphoma Cells," *Asian Pacific Journal of Tropical Disease* 4 (2014): S415–S420, https://doi.org/10.1016/s2222-1808(14)60480-1.

[20] S. Sreelatha, P. R. Padma, and M. Umadevi, "Protective Effects of *Coriandrum sativum* Extracts on Carbon Tetrachloride-Induced Hepatotoxicity in Rats," *Food and Chemical Toxicology* 47, no. 4 (2009): 702–708, https://doi.org/10.1016/j.fct.2008.12.022.

[21] S. Ekin, H. Kiziltas, M. Bayramoglu Akkoyun, et al., "Nephroprotective Effect of *Ferulago angulata* Flowers on *N*-Nitrosodimethylamine-Induced Nephrotoxicity in Rats and its Phytochemical Profile," *Journal of Food Biochemistry* 43, no. 11 (2019): e13030, https://doi.org/10.1111/jfbc.13030.

[22] F. Golfakhrabadi, M. R. Shams Ardekani, S. Saeidnia, et al., "Phytochemical Analysis, Antimicrobial, Antioxidant Activities and Total Phenols of *Ferulago carduchorum* in Two Vegetative Stages (Flower and Fruit)," *Pakistan Journal of Pharmaceutical Sciences* 29, no. 2 (2016): 623–628.

[23] Y. Shokoohinia, S. E. Sajjadi, M. Jamali, G. Abdi, B. Shahbazi, and A. Fattahi, "Antiproliferative Evaluation of Terpenoids and Terpenoid Coumarins From *Ferulago macrocarpa* (Fenzl) Boiss. Fruits," *Pharmacognosy Research* 7, no. 4 (2015): 322–328, https://doi.org/10.4103/0974-8490.158437.

[24] N. Badalamenti, A. Vaglica, A. Maggio, and M. Bruno, "A New Ferulol Derivative Isolated From the Aerial Parts of *Ferulago nodosa* (L.) Boiss. Growing in Sicily (Italy)," *Natural Product Research* 37, no. 19 (2023): 3290–3296, https://doi.org/10.1080/14786419.2022.2074995.

[25] N. Badalamenti, A. Vaglica, A. Porrello, et al., "Phytochemical Investigation and Antitumor Activity of Coumarins From Sicilian Accession of *Ferulago nodosa* (L.) Boiss. Roots," *Natural Product Research* 38, no. 6 (2024): 1024–1035, https://doi.org/10.1080/14786419.2023.2213808.

[26] R. Alkhatib, T. Hennebelle, V. Roumy, et al., "Coumarins, Caffeoyl Derivatives and a Monoterpenoid Glycoside From *Ferulago asparagifolia*," *Biochemical Systematics and Ecology* 37, no. 3 (2009): 230–233, https://doi.org/10.1016/j.bse.2009.03.003.

[27] E. Mongelli, J. Coussio, G. Ciccia, et al., "Studies on the Biological Activity and Chemical Constituents of *Bolax gummifera* (Lam.) Sprengel," *Acta Horticulturae* 501 (1999): 181–184, https://doi.org/10.17660/actahortic.1999.501.27.

[28] F. Wang, D. S. Zhou, G. Z. Wei, F. C. Ren, and J. K. Liu, "Chlorantholides A–F, Eudesmane-type Sesquiterpene Lactones from *Chloranthus elatior*," *Phytochemistry* 77 (2012): 312–317, https://doi.org/10.1016/j.phytochem.2012.02.008.

[29] A. Venditti, A. Bianco, M. Bruno, M. Ben Jemia, and M. Nicoletti, "Phytochemical Study of *Cistus libanotis* L," *Natural Product Research* 29, no. 2 (2015): 189–192, https://doi.org/10.1080/14786419.2014.968569.

[30] E. Maldonado, Ma. Apan, and A. Pérez-Castorena, "Anti-Inflammatory Activity of Phenyl Propanoids From *Coreopsis mutica* Var. *Mutica*," *Planta Medica* 64, no. 07 (1998): 660–661, https://doi.org/10.1055/s-2006-957544.

[31] V. M. Hernández, R. Miranda, M. Martínez, and P. Joseph-Nathan, "Presence of Bornyl *P*-Coumarate in the Roots of *Eupatorium deltoideum*," *Journal of Natural Products* 49, no. 6 (1986): 1173–1174, https://doi.org/10.1021/np50048a059.

[32] C. Herrera, V. Morocho, G. Vidari, C. Bicchi, and G. Gilardoni, "Phytochemical Investigation of Male and Female *Hedyosmum scabrum* (Ruiz & Pav.) Solms Leaves From Ecuador," *Chemistry and Biodiversity* 15, no. 2 (2018): e1700423, https://doi.org/10.1002/cbdv.201700423.

[33] W. Li, Z. Wu, Y. Xia, et al., "Antiviral and Antioxidant Components From the Fruits of *Illicium verum* Hook.F. (Chinese Star Anise)," *Journal of Agricultural and Food Chemistry* 70, no. 12 (2022): 3697–3707, https://doi.org/10.1021/acs.jafc.1c08376.

[34] T. T. M. Nguyen, T. T. Nguyen, H. S. Lee, B. M. Lee, B. S. Min, and J. A. Kim, "Anti-Allergic and Cytotoxic Effects of Sesquiterpenoids and Phenylpropanoids Isolated From *Magnolia Biondii*," *Natural Product Communications* 12, no. 10 (2017): 1543–1545, https://doi.org/10.1177/1934578x1701201005.

[35] S. Xianjin, S. Sha, M. Qi, et al., "Terpenoids From the Barks of *Magnolia Maudiae* (Dunn) Figlar," *Natural Product Research* 32 (2018): 1518–1524, https://doi.org/10.1080/14786419.2017.1385012.

[36] M. J. Cheng, W. L. Lo, J. C. Huang, et al., "Isolation of a New Monoterpenic Ester From the Leaves of *Michelia compressa* (Maxim.) Sargent Var. *Formosana* Kanehira (Magnoliaceae)," *Natural Product Research* 24, no. 7 (2010): 682–686, https://doi.org/10.1080/14786410903281774.

[37] M. K. Langat, A. Helfenstein, C. Horner, et al., "Pumilol, a Diterpenoid With a Rare Strobane Skeleton From *Pinus pumila* (Pinaceae)," *Chemistry and Biodiversity* 15, no. 10 (2018): e1800056, https://doi.org/10.1002/cbdv.201800056.

[38] T. R. Morais, T. A. Costa-Silva, D. D. Ferreira, et al., "Antitrypanosomal Activity and Effect in Plasma Membrane Permeability of (−)-bornyl *P*-Coumarate Isolated From *Piper cernuum* (Piperaceae)," *Bioorganic Chemistry* 89 (2019): 103001, https://doi.org/10.1016/j.bioorg.2019.103001.

[39] J. Glaser, M. Schultheis, H. Moll, B. Hazra, and U. Holzgrabe, "Antileishmanial and Cytotoxic Compounds From *Valeriana wallichii* and Identification of a Novel Nepetolactone Derivative," *Molecules* 20, no. 4 (2015): 5740–5753, https://doi.org/10.3390/molecules20045740.

[40] V. G. S. Box and W. R. Chan, "Terpenoids From *Verbesina rupestris*," *Phytochemistry* 14, no. 2 (1975): 583, https://doi.org/10.1016/0031-9422(75)85137-5.

[41] A. Arciniegas, A. L. Pérez-Castorena, J. L. Villaseñor, and A. Romo de Vivar, "Cadinenes and Other Metabolites From *Verbesina sphaerocephala* A. Gray," *Biochemical Systematics and Ecology* 93 (2020): 104183.

[42] I. V. Ogungbe, R. A. Crouch, W. A. Haber, and W. N. Setzer, "Phytochemical Investigation of *Verbesina turbacensis* Kunth: Trypanosome Cysteine Protease Inhibition by (-)-bornyl Esters," *Natural Product Communications* 5, no. 8 (2010): 1161–1166, https://doi.org/10.1177/1934578x1000500801.

[43] M. Hekmati, S. Hasanirad, A. Khaledi, and D. Esmaeili, "Green Synthesis of Silver Nanoparticles Using Extracts of *Allium rotundum* L, *Falcaria vulgaris* Bernh, and *Ferulago angulata* Boiss, and Their Antimicrobial Effects *In Vitro*," *Gene Reports* 19 (2020): 100589, https://doi.org/10.1016/j.genrep.2020.100589.

[44] M. Huang, J. J. Lu, and J. Ding, "Natural Products in Cancer Therapy: Past, Present and Future," *Natural products and bioprospecting* 11, no. 1 (2021): 5–13, https://doi.org/10.1007/s13659-020-00293-7.

[45] S. C. Gupta, J. H. Kim, S. Prasad, and B. B. Aggarwal, "Regulation of Survival, Proliferation, Invasion, Angiogenesis, and Metastasis of Tumor Cells Through Modulation of Inflammatory Pathways by Nutraceuticals," *Cancer and Metastasis Reviews* 29, no. 3 (2010): 405–434, https://doi.org/10.1007/s10555-010-9235-2.

[46] S. Fulda, "Modulation of Apoptosis by Natural Products for Cancer Therapy," *Planta Medica* 76, no. 11 (2010): 1075–1079, https://doi.org/10.1055/s-0030-1249961.

[47] M. K. Kim, K. Kim, J. Y. Han, J. M. Lim, and Y. S. Song, "Modulation of Inflammatory Signaling Pathways by Phytochemicals in Ovarian Cancer," *Genes & Nutrition* 6, no. 2 (2011): 109–115, https://doi.org/10.1007/s12263-011-0209-y.

[48] D. Trachootham, J. Alexandre, and P. Huang, "Targeting Cancer Cells by ROS-Mediated Mechanisms: A Radical Therapeutic Approach?" *Nature Reviews Drug Discovery* 8, no. 7 (2009): 579–591, https://doi.org/10.1038/nrd2803.

[49] A. Attanzio, L. Tesoriere, M. Allegra, and M. A. Livrea, "Monofloral Honeys by Sicilian Black Honeybee (*Apis mellifera* Ssp. *Sicula*) Have High Reducing Power and Antioxidant Capacity," *Heliyon* 2, no. 11 (2016): e00193, https://doi.org/10.1016/j.heliyon.2016.e00193.

[50] A. Attanzio, A. D'Anneo, F. Pappalardo, et al., "Phenolic Composition of Hydrophilic Extract of Manna From Sicilian *Fraxinus angustifolia* Vahl and its Reducing, Antioxidant and Anti-Inflammatory Activity *In Vitro*," *Antioxidants* 8, no. 10 (2019): 494, https://doi.org/10.3390/antiox8100494.

[51] G. Culletta, M. Allegra, A. M. Almerico, I. Restivo, and M. Tutone, "In Silico Design, Synthesis, and Biological Evaluation of Anticancer Arylsulfonamide Endowed With Anti-Telomerase Activity," *Pharmaceuticals* 15, no. 1 (2022): 82, https://doi.org/10.3390/ph15010082.

[52] I. Restivo, L. Tesoriere, A. Frazzitta, M. A. Livrea, A. Attanzio, and M. Allegra, "Anti-Proliferative Activity of A Hydrophilic Extract of Manna From Fraxinus Angustifolia Vahl Through Mitochondrial Pathway-Mediated Apoptosis and Cell Cycle Arrest in Human Colon Cancer Cells," *Molecules* 25, no. 21 (2020): 5055, https://doi.org/10.3390/molecules25215055.

[53] A. Cilla, G. López-García, R. Barberá, et al., "Antiproliferative Effects of Bioaccessible Fractions of Honeys From Sicilian Black Honeybee (*Apis mellifera* Ssp. *Sicula*) on Human Colorectal Carcinoma Cells," *International Journal of Food Science and Technology* 57 (2022): 2636–2645.

[54] M. Allegra, A. D'Anneo, A. Frazzitta, et al., "The Phytochemical Indicaxanthin Synergistically Enhances Cisplatin-Induced Apoptosis in HeLa Cells via Oxidative Stress-Dependent P53/p21waf1 Axis," *Biomolecules* 10, no. 7 (2020): 994, https://doi.org/10.3390/biom10070994.

[55] I. Restivo, A. Attanzio, L. Tesoriere, M. Allegra, G. Garcia-Llatas, and A. Cilla, "A Mixture of Dietary Plant Sterols at Nutritional Relevant Serum Concentration Inhibits Extrinsic Pathway of Eryptosis Induced by Cigarette Smoke Extract," *International Journal of Molecular Sciences* 24, no. 2 (2023): 1264, https://doi.org/10.3390/ijms24021264.

[56] I. Restivo, M. G. Basilicata, I. C. Giardina, et al., "A Combination of Polymethoxyflavones From Citrus Sinensis and Prenylflavonoids From Humulus Lupulus Counteracts IL-1β-Induced Differentiated Caco-2 Cells Dysfunction via a Modulation of NF-κB/Nrf2 Activation," *Antioxidants* 12, no. 8 (2023): 1621, https://doi.org/10.3390/antiox12081621.

[57] M. Ghasemi, T. Turnbull, S. Sebastian, and I. Kempson, "The MTT Assay: Utility, Limitations, Pitfalls, and Interpretation in Bulk and Single-Cell Analysis," *International Journal of Molecular Sciences* 22, no. 23 (2021): 12827, https://doi.org/10.3390/ijms222312827.

[58] G. Indrayanto, G. S. Putra, and F. Suhud, "Validation of *In-Vitro* Bioassay Methods: Application in Herbal Drug Research," *Profiles of Drug Substances, Excipients and Related Methodology* 46 (2021): 273–307, https://doi.org/10.1016/bs.podrm.2020.07.005.

[59] J. P. Ondo, J. B. Lekana-Douki, J. B. Bongui, et al., "*In Vitro* Antiplasmodial Activity and Cytotoxicity of Extracts and Fractions of *Vitex madiensis*, Medicinal Plant of Gabon," *Tropical Medicine and International Health: TM & IH* 17, no. 3 (2012): 316–321, https://doi.org/10.1111/j.1365-3156.2011.02922.x.

[60] D. F. Smee, B. L. Hurst, W. J. Evans, et al., "Evaluation of Cell Viability Dyes in Antiviral Assays With RNA Viruses that Exhibit Different Cytopathogenic Properties," *Journal of Virological Methods* 246 (2017): 51–57, https://doi.org/10.1016/j.jviromet.2017.03.012.

[61] M. T. Gomes, K. Palasiewicz, V. Gadiyar, et al., "Phosphatidylserine Externalization by Apoptotic Cells is Dispensable for Specific Recognition Leading to Innate Apoptotic Immune Responses," *Journal of Biological Chemistry* 298, no. 7 (2022): 102034, https://doi.org/10.1016/j.jbc.2022.102034.

[62] S. Miwa, S. Kashyap, E. Chini, and T. von Zglinicki, "Mitochondrial Dysfunction in Cell Senescence and Aging," *The Journal of Clinical Investigation* 132, no. 13 (2022): e158447, https://doi.org/10.1172/jci158447.

[63] D. L. Vaux, "Apoptogenic Factors Released From Mitochondria," *Biochimica et Biophysica Acta (BBA)-Molecular Cell Research* 1813, no. 4 (2011): 546–550, https://doi.org/10.1016/j.bbamcr.2010.08.002.

[64] J. F. Passos, G. Nelson, C. Wang, et al., "Feedback Between P21 and Reactive Oxygen Production is Necessary for Cell Senescence," *Molecular Systems Biology* 6, no. 1 (2010): 347, https://doi.org/10.1038/msb.2010.5.

[65] M. Redza-Dutordoir and D. A. Averill-Bates, "Activation of Apoptosis Signalling Pathways by Reactive Oxygen Species," *Biochimica et Biophysica Acta (BBA)-Molecular Cell Research* 1863, no. 12 (2016): 2977–2992, https://doi.org/10.1016/j.bbamcr.2016.09.012.

[66] N. Sun, R. J. Youle, and T. Finkel, "The Mitochondrial Basis of Aging," *Molecular Cell* 61, no. 5 (2016): 654–666, https://doi.org/10.1016/j.molcel.2016.01.028.

[67] J. Ježek, K. F. Cooper, and R. Strich, "Reactive Oxygen Species and Mitochondrial Dynamics: The Yin and Yang of Mitochondrial Dysfunction and Cancer Progression," *Antioxidants* 7, no. 1 (2018): 13, https://doi.org/10.3390/antiox7010013.

[68] G. E. Villalpando-Rodriguez and S. B. Gibson, "Reactive Oxygen Species (ROS) Regulates Different Types of Cell Death by Acting as a Rheostat," *Oxidative Medicine and Cellular Longevity* 2021, no. 1 (2021): 9912436, https://doi.org/10.1155/2021/9912436.

[69] C. Wang and R. J. Youle, "The Role of Mitochondria in Apoptosis," *Annual Review of Genetics* 43, no. 1 (2009): 95–118, https://doi.org/10.1146/annurev-genet-102108-134850.

[70] T. Miyashita, S. Krajewski, M. Krajewska, et al., "Tumor Suppressor P53 is a Regulator of Bcl-2 and Bax Gene Expression *In Vitro* and *In Vivo*," *Oncogene* 9, no. 6 (1994): 1799–1805.

[71] N. N. Kreis, F. Louwen, and J. Yuan, "The Multifaceted P21 (Cip1/Waf1/CDKN1A) in Cell Differentiation, Migration and Cancer Therapy," *Cancers* 11, no. 9 (2019): 1220, https://doi.org/10.3390/cancers11091220.

[72] D. P. Xu, Y. Li, X. Meng, et al., "Natural Antioxidants in Foods and Medicinal Plants: Extraction, Assessment and Resources," *International Journal of Molecular Sciences* 18, no. 1 (2017): 96, https://doi.org/10.3390/ijms18010096.

[73] A. Masyita, R. Mustika Sari, A. Dwi Astuti, et al., "Terpenes and Terpenoids as Main Bioactive Compounds of Essential Oils, Their Roles in Human Health and Potential Application as Natural Food Preservatives," *Food Chemistry X* 13 (2022): 100217, https://doi.org/10.1016/j.fochx.2022.100217.

[74] C. Y. Wang, Y. W. Chen, and C. Y. Hou, "Antioxidant and Antibacterial Activity of Seven Predominant Terpenoids," *International Journal of Food Properties* 22, no. 1 (2019): 230–238, https://doi.org/10.1080/10942912.2019.1582541.

[75] I. Potočnjak, I. Gobin, and R. Domitrović, "Carvacrol Induces Cytotoxicity in Human Cervical Cancer Cells But Causes Cisplatin Resistance: Involvement of MEK-ERK Activation," *Phytotherapy Research* 32, no. 6 (2018): 1090–1097, https://doi.org/10.1002/ptr.6048.

[76] P. Wróblewska-Łuczka, J. Cabaj, J. Bargieł, and J. J. Łuszczki, "Anticancer Effect of Terpenes: Focus on Malignant Melanoma," *Pharmacological Reports* 75, no. 5 (2023): 1115–1125, https://doi.org/10.1007/s43440-023-00512-1.

[77] P. Kłos and D. Chlubek, "Plant-Derived Terpenoids: A Promising Tool in the Fight Against Melanoma," *Cancers*. 14, no. 3 (2022): 502, https://doi.org/10.3390/cancers14030502.

[78] M. Di Martile, S. Garzoli, M. Sabatino, et al., "Antitumor Effect of Melaleuca Alternifolia Essential Oil and Its Main Component Terpinen-4-Ol in Combination With Target Therapy in Melanoma Models," *Cell Death Discovery* 7, no. 1 (2021): 127, https://doi.org/10.1038/s41420-021-00510-3.

[79] Y. E. Yoon, Y. J. Jung, and S. J. Lee, "The Anticancer Activities of Natural Terpenoids That Inhibit Both Melanoma and Non-Melanoma Skin Cancers," *International Journal of Molecular Sciences* 25, no. 8 (2024): 4423, https://doi.org/10.3390/ijms25084423.

[80] Z. Balavandi, A. Neshasteh-Riz, F. Koosha, S. Eynali, M. Hoormand, and M. Shahidi, "The Use of *SS*-Elemene to Enhance Radio Sensitization of A375 Human Melanoma Cells," *Cell J* 21, no. 4 (2020): 419–425, https://doi.org/10.22074/cellj.2020.6326.

[81] M. Platzer, S. Kiese, T. Herfellner, U. Schweiggert-Weisz, O. Miesbauer, and P. Eisner, "Common Trends and Differences in Antioxidant Activity Analysis of Phenolic Substances Using Single Electron Transfer Based Assays," *Molecules* 26, no. 5 (2021): 1244, https://doi.org/10.3390/molecules26051244.

[82] K. A. Wojtunik-Kulesza, Ł. M. Cieśla, and M. Waksmundzka-Hajnos, "Approach to Determination a Structure–Antioxidant Activity Relationship of Selected Common Terpenoids Evaluated by ABTS•+ Radical Cation Assay," *Natural Product Communications* 13, no. 3 (2018): 308, https://doi.org/10.1177/1934578x1801300308.

[83] D. Trachootham, W. Lu, M. A. Ogasawara, N. R. D. Valle, and P. Huang, "Redox Regulation of Cell Survival," *Antioxidants and Redox Signaling* 10, no. 8 (2008): 1343–1374, https://doi.org/10.1089/ars.2007.1957.

[84] M. Schieber and N. S. Chandel, "ROS Function in Redox Signaling and Oxidative Stress," *Current Biology* 24, no. 10 (2014): R453–R462, https://doi.org/10.1016/j.cub.2014.03.034.

[85] C. Gorrini, I. S. Harris, and T. W. Mak, "Modulation of Oxidative Stress as an Anticancer Strategy," *Nature Reviews Drug Discovery* 12, no. 12 (2013): 931–947, https://doi.org/10.1038/nrd4002.

[86] C. C. Su, J. G. Lin, T. M. Li, et al., "Curcumin-Induced Apoptosis of Human Colon Cancer Colo 205 Cells Through the Production of ROS, Ca2+ and the Activation of Caspase-3," *Anticancer Research* 26, no. 6 (2006): 4379–4389.

[87] S. C. Gupta, S. Patchva, W. Koh, and B. B. Aggarwal, "Discovery of Curcumin, a Component of Golden Spice, and its Miraculous Biological Activities," *Clinical and Experimental Pharmacology and Physiology* 39, no. 3 (2012): 283–299, https://doi.org/10.1111/j.1440-1681.2011.05648.x.

[88] S. Fulda, "Resveratrol and Derivatives for the Prevention and Treatment of Cancer," *Drug Discovery Today* 15, no. 17-18 (2010): 757–765, https://doi.org/10.1016/j.drudis.2010.07.005.

[89] R. Gogada, V. Prabhu, M. Amadori, R. Scott, S. Hashmi, and D. Chandra, "Resveratrol Induces P53-Independent, X-Linked Inhibitor of Apoptosis Protein (XIAP)-Mediated Bax Protein Oligomerization on Mitochondria to Initiate Cytochrome C Release and Caspase Activation," *Journal of Biological Chemistry* 286, no. 33 (2011): 28749–28760, https://doi.org/10.1074/jbc.m110.202440.

[90] L. Raj, T. Ide, A. U. Gurkar, et al., "Selective Killing of Cancer Cells by a Small Molecule Targeting the Stress Response to ROS," *Nature* 475, no. 7355 (2011): 231–234, https://doi.org/10.1038/nature10167.

[91] X. Chen, Y. Zhao, W. Luo, et al., "Celastrol Induces ROS-Mediated Apoptosis via Directly Targeting Peroxiredoxin-2 in Gastric Cancer Cells," *Theranostics* 10, no. 22 (2020): 10290–10308, https://doi.org/10.7150/thno.46728.

[92] S. Park, W. Lim, S. You, and G. Song, "Ochratoxin A Exerts Neurotoxicity in Human Astrocytes Through Mitochondria-Dependent Apoptosis and Intracellular Calcium Overload," *Toxicology Letters* 313 (2019): 42–49, https://doi.org/10.1016/j.toxlet.2019.05.021.

[93] W. Park, S. Park, G. Song, and W. Lim, "Inhibitory Effects of Osthole on Human Breast Cancer Cell Progression via Induction of Cell Cycle Arrest, Mitochondrial Dysfunction, and ER Stress," *Nutrients* 11, no. 11 (2019): 2777, https://doi.org/10.3390/nu11112777.

[94] J. Y. Chuang, Y. F. Huang, H. F. Lu, et al., "Coumarin Induces Cell Cycle Arrest and Apoptosis in Human Cervical Cancer HeLa Cells Through a Mitochondria- and Caspase-3 Dependent Mechanism and NF-kappaB Down-Regulation," *In Vivo (Athens, Greece)* 21, no. 6 (2007): 1003–1009.

[95] P. K. Raut, H. S. Lee, S. H. Joo, and K. S. Chun, "Thymoquinone Induces Oxidative Stress-Mediated Apoptosis Through Downregulation of Jak2/STAT3 Signaling Pathway in Human Melanoma Cells," *Food and Chemical Toxicology* 157 (2021): 112604, https://doi.org/10.1016/j.fct.2021.112604.

[96] J. J. De La Chapa, P. K. Singha, D. R. Lee, and C. B. Gonzales, "Thymol Inhibits Oral Squamous Cell Carcinoma Growth via Mitochondria-Mediated Apoptosis," *Journal of Oral Pathology & Medicine* 47, no. 7 (2018): 674–682, https://doi.org/10.1111/jop.12735.

[97] S. Bardon, V. Foussard, S. Fournel, and A. Loubat, "Monoterpenes Inhibit Proliferation of Human Colon Cancer Cells by Modulating Cell Cycle-Related Protein Expression," *Cancer Letters* 181, no. 2 (2002): 187–194, https://doi.org/10.1016/s0304-3835(02)00047-2.

[98] Y. Li, J. M. Wen, C. J. Du, et al., "Thymol Inhibits Bladder Cancer Cell Proliferation via Inducing Cell Cycle Arrest and Apoptosis," *Biochemical and Biophysical Research Communications* 491, no. 2 (2017): 530–536, https://doi.org/10.1016/j.bbrc.2017.04.009.

[99] D. A. Foster, P. Yellen, L. Xu, and M. Saqcena, "Regulation of G1 Cell Cycle Progression: Distinguishing the Restriction

Point From a Nutrient-Sensing Cell Growth Checkpoint(s)," *Genes & Cancer* 1, no. 11 (2010): 1124–1131, https://doi.org/10.1177/1947601910392989.

[100] S. Vyas, E. Zaganjor, and M. C. Haigis, "Mitochondria and Cancer," *Cell.* 166, no. 3 (2016): 555–566, https://doi.org/10.1016/j.cell.2016.07.002.

[101] N. Yadav, R. Gogada, J. O'Malley, et al., "Molecular Insights on Cytochrome C and Nucleotide Regulation of Apoptosome Function and Its Implication in Cancer," *Biochimica et Biophysica Acta* 1867, no. 1 (2020): 118573.

[102] Y. Shen and E. White, "p53-Dependent Apoptosis Pathways," *Advances in Cancer Research* 82 (2001): 55–84, https://doi.org/10.1016/s0065-230x(01)82002-9.

[103] K. A. Manu and G. Kuttan, "Ursolic Acid Induces Apoptosis by Activating P53 and Caspase-3 Gene Expressions and Suppressing NF-Kb Mediated Activation of Bcl-2 in B16F-10 Melanoma Cells," *International Immunopharmacology* 8, no. 7 (2008): 974–981, https://doi.org/10.1016/j.intimp.2008.02.013.